4-2017

Towards a cost-effective biorefinery : production of activated carbons from residual biomass for energy storage devices.

Zachary Dean Herde
University of Louisville

TOWARDS A COST-EFFECTIVE BIOREFINERY: PRODUCTION OF ACTIVATED CARBONS FROM RESIDUAL BIOMASS FOR ENERGY STORAGE DEVICES

By

Zachary Dean Herde
B.S., University of Louisville, 2016

A Thesis
Submitted to the Faculty of the
University of Louisville
J.B. Speed School of Engineering
as Partial Fulfillment of the Requirements
for the Professional Degree

MASTER OF ENGINEERING

Department of Chemical Engineering

April 2017

TOWARDS A COST-EFFECTIVE BIOREFINERY: PRODUCTION OF ACTIVATED CARBONS FROM RESIDUAL BIOMASS FOR ENERGY STORAGE DEVICES

Submitted by: _____

Zachary Dean Herde

A Thesis Approved On

_____

(Date)

by the Following Reading and Examination Committee:

_____

Dr. R. Eric Berson, Thesis Director

_____

Dr. Noppadon Sathitsuksanoh

_____

Dr. Gamini Sumanasekera

ACKNOWLEDGEMENTS

First and foremost, I would like to thank Dr. Jagannadh Satyavolu for his unwavering support, his teaching, and his guidance throughout the past three years. Without him I know I would not be where I am today in research and in life.

I would like to thank my committee, Dr. Eric Berson for his teaching, his advice and guidance while writing this thesis. Dr. Gamini Sumanasekera for his guidance and support in all of my research endeavors over the years, including the research involved in writing this thesis. Dr. Noppadon Sathitsuksanoh for his support and willingness to help when it comes to class, graduate school, and being on my committee.

I would also like to thank Dr. Mahendra Sunkara and the Conn Center for Renewable Energy Research for providing me the opportunity and resources required to pursue research when those kinds of opportunities seemed limited. This extends to all related professors, students, and staff involved in my research here.

I would like to thank Drs. Michael and Carole Graetzel, Mr. and Mrs. Xavier and Diane Burrus, and EPFL for providing me a life-changing research experience and increasing my scientific and cultural awareness.

I would like to thank the Brown-Forman Corporation for their material and financial support and MeadWestVaco for their material samples.

I would like to thank all of my teachers, co-workers, mentors, and collaborators past, present, involved in this work, and in my life outside of it.

And finally, thank you to my family and friends, who have always encouraged and supported me when I have had misgivings about my own abilities; and who inspire me every day to do good work that will further humanity toward a world worthy of their kindness and compassion.

ABSTRACT

Waste from agricultural processing provides material from which bio-based fuels and products can be extracted and produced in biorefineries. However, transport, processing, and production from these sources is not yet cost-effective for mass production. Co-product strategies that create valuable by-products need to be developed and implemented for biorefineries to become viable.

High surface area activated carbon fibers for energy storage purposes were produced and characterized as part of a co-product strategy for dried distiller's grains (DDG) and soy-based biorefineries. The data shows that hydrolysis is necessary to produce carbons from both DDG and soy hulls with sufficient surface areas. Carbon surface area from hydrolyzed DDG reached 1700 m^2/g and from hydrolyzed soy hulls reached 1300 m^2/g. Average pore size width was 2.92 nm for DDG and 2.20 nm for soy hulls. In comparison, carbons from non-hydrolyzed DDG and soy hulls had surface areas of 10 m^2/g and 690 m^2/g, and average pore size widths of 9.53 nm and 2.67 nm. The physical manifestation of these numbers was visualized with SEM and TEM imaging.

Double layer supercapacitors made from the carbons showed capacitances of 100 F/g, the expected value for standard supercapacitors made with activated carbon materials. When implemented as a carbon layer in perovskite solar cells, the device was not efficient, but when used as an additive in the ZrO layer, photo conversion efficiencies improved from 9 to 12%. When used with specific solvent and oil mixtures, the carbons can be efficiently deposited on membranes and used to trap hydrogen gas in their pores for low pressure storage, benefiting applications such as hydrogen powered vehicles.

Techno-economic analysis showed that carbonization processes with a max yield of 42% can achieve profits that aid in biorefinery costs and that this revenue increases with larger capacity throughput. The analysis projects that these profits will vary from approximately $3.7 million for 25,000 tonnes of DDG processed per year to $87 million for a plant that processes 500,000 tonnes of DDG per year.

Table of Contents

NOMENCLATURE

AM – air mass

atm – atmosphere

C – capacitance

cm – centimeter

°C – degrees Celsius

ε – dielectric constant

F – Farad

g – gram

gal – gallon

K - Kelvin

kg – kilogram

km – kilometer

kPa - kilopascals

L – liter

M – molarity

m – meter

mA – milliamps

MJ - megajoules

mL - milliliter

mm – millimeter

μm - micrometer

nm – nanometer

psi – pounds per square inch

V - volt

W – watt

wt – weight

yr - year

LIST OF ABBREVIATIONS

AC – Activated Carbons

BET – Brunauer-Emmett-Teller

C5 – Five carbon sugar

DDG – Dried Distiller's Grains

DI - deionized

DOE – Department of Energy

EDAX – energy dispersive analysis via x-ray

EDLC – electrochemical double layer capacitor

FTO – Fluorine doped Tin Oxide

G - global

HTM – hole transport medium

IUPAC – International Union of Pure and Applied Chemistry

IV – current density vs. voltage

MWV – MeadWestVaco Corporation

No. - number

NOx – Nitrogen oxide pollutants

PCE – photo conversion efficiency

PTFE – Polytetrafluoroethylene

SEM – scanning electron microscopy

SOx – Sulfur oxide pollutants

TCO – transparent conducting oxide

TEM – transmission electron microscopy

USDA – United States Department of Agriculture

LIST OF TABLES

LIST OF FIGURES

LIST OF EQUATIONS

I. INTRODUCTION

Biorefineries are taking a more prevalent role in society as humanity looks to plants to provide bio based products, commodities, and liquid fuel replacements. Many biomass sources, including corn, grasses, sorghum, soy, hemp, kenaf, coconut, plantain, and a variety of others have all shown promise as product precursors in a biorefinery setting. However, the extraction and refining of the materials to obtain precursors are difficult to complete as compounds such as lignin, cellulose, and hemicellulose require high temperatures and pressures to process. In order to create biorefineries that are economically viable, techno-economic analyses have pointed toward the production of value-added co-products as ways to create added income that supplement the high expense that comes with processing biomasses in this way. These co-products ideally add little capital or operating costs, but are high-value in the market; allowing for revenue that off-sets the overall cost of the refinery. The way these products are produced also has a large impact on the viability of the co-product strategy. Therefore, simple processes with little energy or materials costs ultimately benefit the most.

In an attempt to resolve this, research has explored the potential array of co-products that can come from leftover biomass after initial fermentation and distillation. One co-product involves the separation of a nutrient-rich and fiber-rich fraction. The nutrient-rich fraction can be sold for a small profit back to the agricultural industry. Extraction processes that break-down and remove hemicellulose from the remaining fiber-rich fraction in the form of five carbon sugars such as xylose and arabinose are another option that has been explored. Through a simple, relatively low temperature, and ambient pressure hydrolysis, these sugars can be extracted and utilized in a variety of

situations. These include as precursors to biofuels and precursors for biodegradable green plastics. The sugars can also be used as is, if processed in a way that allows for food-grade classification. The result of this hydrolysis is a stripped down, carbon-rich cellulose structure that could also provide a high-value co-product if taken advantage of properly.

Activated carbons are becoming one of the top materials choices when it comes to energy storage and power devices due to their stability, durability, and conductivity. High efficiencies have been shown in devices such as supercapacitors and photovoltaics. This is extremely helpful to the renewable energy cause as it could allow for storage of renewably produced electricity, solving one of the major issues that has stifled renewable energy implementation for many years. Carbons are also being investigated for their use in solid-state hydrogen storage modules that could provide on-board hydrogen fuel. In this application, vehicular explosion and weight of the vehicle would be drastically reduced compared to current liquid and pressurized gas designs. All of these properties have increased their inherent value as more information is obtained from observation and application of carbons in energy applications.

In the past, activated carbons were made industrially from anthracite precursors, a non-renewable source that requires mining of fossil fuels like coal. Paper and pulp industries have also used their mill products as precursors for activated carbons. Even more recently, lignocellulosic biomasses have been implemented as activated carbon precursors due to their structural qualities that yield carbons that can be tailored to fit specific needs. These needs often involve a high charge capacity, quick charge/discharge cycles, multiple cycle stability, and energy density when packed with a fuel source. This

use of biomass is almost always a direct conversion from the biomass source directly into activated carbons, providing carbon as the only product.

The focus of this research was to create a high-value co-product in the form of activated carbon using residual biomass (dried distiller's grains and soy hulls) from a C-5 sugar extraction refinery process. Specific objectives included characterization of the residual biomass before and after hydrolysis, material characterization of the carbons produced using both pre- and post-hydrolysis biomass, economic analysis of the impact on biorefinery costs, and application of the carbons in energy storage and power devices. These devices included supercapacitors, perovskite solar cells, and hydrogen storage. To accomplish these goals, a standard carbon production procedure was synthesized from published production methods that focused on creating materials with small pore sizes and high surface areas. Procedures were implemented that produced the desired characteristics for energy storage applications. The resulting carbons were then analyzed for surface areas, pore size distribution, adsorption capabilities, and elemental composition. Techno-economic models were developed to determine the impact of production and sale of activated carbons in a large-scale biorefinery using these corn and soy fibers as precursor materials.

II. REVIEW OF LITERATURE

A. THE CHEMICAL STRUCTURE OF BIOMASS

Biomass, organic material that is derived from plants or animals, as an energy source has become a key staple in the fight against using fossil fuels [Kirk-Othmer, 2007]. Biomass can either be used as is, or through processing and refining. This is typically in the form of heat through the burning of biomass or fuel alcohols via fermentation of storage and structural sugars. These sugar compounds and proteins are abundant in biomasses in the forms of long polymer chains that comprise the structure of the plant. These chains are formed via the following photosynthesis reaction.

$$CO_2 + H_2O + light + chlorophyll \rightarrow (CH_2O) + O_2 \quad (1)$$

The carbohydrates produced are an example of energy conversion in that plants can produce high-energy compounds from a photochemical process with low conversion efficiency. Regardless, the compounds made are mainly lignin, cellulose, and hemicellulose. Lignin is a protein chain that provides the "glue" of the plant structure, nestled between the cell walls formed from the other two compounds. It also permits and assists in the vascular conduction of water throughout the plant system. Cellulose is the main structural component of the majority of plants. It is a straight chain, crystalline material made up of hundreds to thousands of D-Glucose rings linked in polymeric form. Cellulose provides the main structure for the cell wall in green plants. In conjunction with

cellulose, hemicellulose, made of varying levels of glucose, arabinose, xylose, mannose, and dextrose, is another high bond energy compound. This material, like cellulose, forms long chains, but is typically branched [Campbell, 2013]. Current biofuels research focuses on the extraction and processing of biomass in order to obtain and utilize the energy stored in the chemical bonds of these various compounds. However, their material strength can make both processing and refining difficult.

B. INTEGRATED BIO-REFINERY CONCEPTS AND ECONOMICS

Biomass as a source of fuel is dependent on the sugar content of the fiber being used. In most fuel ethanol cases, starches within the corn are the target. This is similar to beverage alcohol production in that enzymes are used to break down starch chains, followed by a fermentation process, and then refinement by distillation to produce ethanol not suitable for drinking, but rather as an additive to car engines. This has many inherent problems, the biggest concern being the use of a nutritional food product as car fuel. In creating fuel ethanol, there is a decline in available food source corn, driving up prices for both as demand continues to increase due to an increasing global population [Kazi, 2010]. Therefore, many refineries are attempting to ferment sugars from ligno-cellulosic biomasses that are not used as food products and are instead from sustainable, agricultural plant sources. According to some studies, enough lingo-cellulosic biomass is grown cost-effectively and environmentally sustainably to ferment 50 billion gallons of fuel annually [Perlack, 2005]. Most models look at wood as the main source of this biomass. However, in theory, all plant sources in one form or another can provide the

sugars and compounds needed for fuel production, allowing current models to expand beyond that of soft and hard woods. Ligno-cellulosic biomass typically comes with the added benefit of being a waste product from a preceding process. For example, dried distillers grains (DDG) from corn ethanol plants and beverage alcohol distilleries in addition to soy hulls from soy processing are lingo-cellulosic materials that can be utilized to produce biofuels.

While this employment of lingo-cellulosic waste materials aids in reducing the use of food crops, there are still issues that need to be overcome when it comes to the mechanical and chemical processing of the biomass. First, there are potential material losses due to pre-processing. This processing is important as it removes sand, dirt, and other materials that could be harmful to the refinery process. This can be split into three main categories. Fiber preparation loss encompasses losses of material as it is being baled or loaded for transportation. Removal of residual grain and other unusable biomass portions adds to this processing reduction. Finally, there is a storage loss that removes material as it is stored. The constant shuffling of material leads to loosened and smaller material components being left behind. Overall, these losses can result in a 25% reduction in initial material mass [Hurter, 2007]. Another consideration that adds to the overall cost of bio-refineries is the availability of the varying sources of biomass. While sustainable biomass numbers are relatively high, approximately 194 million dry tons per year [Hurter, 2007], the concentration of these materials and resultant need to transport them cross country leads to increased processing cost. Not only would the refinery need to pay for the fuels costs, but as discussed previously, losses due to transportation can reduce the overall amount that is actually transported [Hurter, 2007]. Therefore, locally

available, sustainable biomass materials would be the best type of material as it would reduce all of these pre-processing costs by eliminating extensive transportation and storage needs.

While this focus on local sustainability can reduce some expenses, there are many factors that need to be considered when looking at equipment and utility expenses (Figure 2.1). When processing materials that contain lignin (lingo-cellulosic biomass), high pressures and temperatures are required to extract any beneficial chemicals from the material for biofuel production. These increased processing values can add to the overall production cost, driving up prices of the finished fuels [Kazi, 2010]. 40-70% of the total production cost is dependent on the biomass transportation and processing alone [Cardona, 2007; Solomon, 2007].

TABLE I

FEEDSTOCK COMPOSITION AND PROCESS CONDITIONS [Sierra, 2008]

Biomass Feedstock	Residence Time	Temperature	Pressure
Low Lignin Content (12-18%)	1-2 Hours	100-120 ˚C	1-2 atm
Medium Lignin Content (18-24%)	~ 30 days	~ 55˚C	1 atm
High Lignin Content (>24%)	~ 2 hours	~ 150 ˚C	15 atm

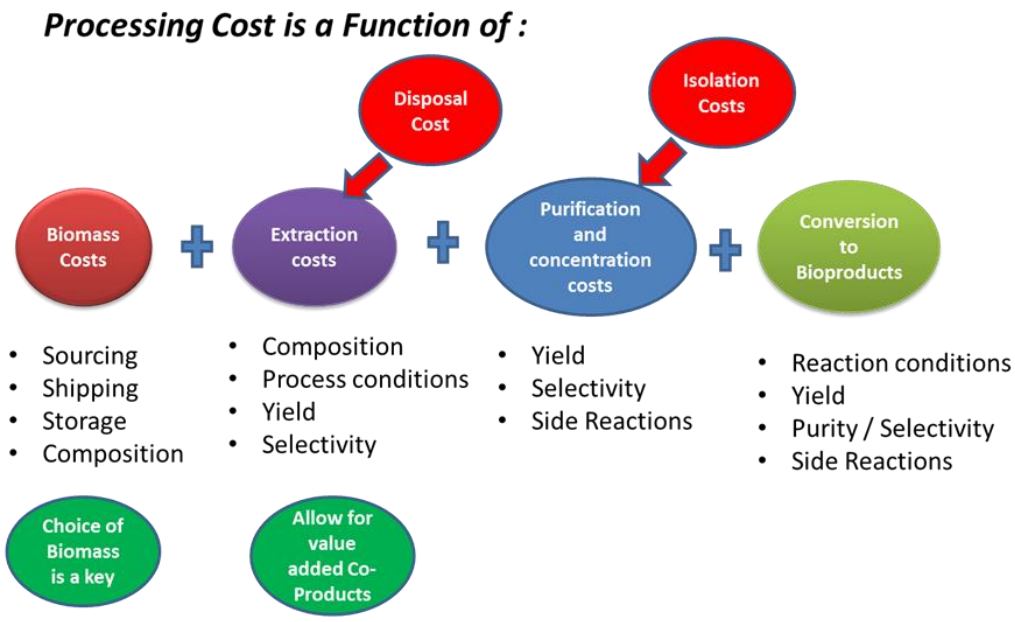

FIGURE 2.1 - Cost breakdown of bio-refinery processing [Fonseca, 2014]

Therefore, selection of biomass based on composition is also a key component of creating a bio-refinery that is effective at reducing the overall cost of the production of biofuels. Materials with inherently less lignin are able to release their sugars and fuel products with minimal effort. This is indicated by reductions in process temperatures and pressures (Table I). Corn stover from fuel ethanol plants is considered a good choice for refinery because of its low lignin content and high hemicellulose content compared to other agricultural crops produced and processed in the same volumes. This would apply to any material that is used locally that contains relatively low amounts of lignin. In places that produce lots of waste corn fiber, like Louisville, KY, distillery waste becomes an effective feed stream for a hemicellulosic, five carbon sugar refinery due to its abundance and low initial cost. Many of the aforementioned references presented the idea of co-products as a potential method for lowering costs and improving the overall

economics of the system. This was mainly denoted in one of two forms. The first is as an energy source to help power generators and boilers to run the equipment. While it does help with utility costs, the energy density is not comparable to natural gas and coal. It is also still voluminous, making the transport and burning of it as fodder inefficient in the long run. The second method involves selling the leftover fiber back to farmers as animal feed at a relatively low value. Thus, creating additional co-products from a process or producing higher value co-products can provide a return that provides a sustainable income source. This then relieves initial investment costs and continuous expenditures such as salaries and raw materials costs.

Fonseca et. al [2014] discuss a concept to create an integrated bio-refinery process using dried distiller's grains from distilleries as the initial raw material. Knowing that the material contained a high hemicellulose concentration, they designed a selective hydrolysis process to remove hemicellulose from the corn fiber biomass. This hemicellulose could then be converted to xylose sugar and xylo-derivatives for biofuel use in jets and as a green precursor in plastic production. This process was also shown to greatly increase the surface area of the fiber. Lupitskyy et. al [2014] designed experiments to show that the fiber after the hydrolysis has 113% higher fat content, 15 % higher digestible nutrients, and 15% higher digestible energy. This work suggested that these co-product side streams could be added to animal feed to improve feed quality, allowing for effective cost-utilization of DDG for bio-refinery purposes.

Bio-refineries have recently been a major focus of development, with funding coming from the Department of Energy's Biorefinery Technology Office [DOE, 2017]. These integrated systems are defined as refineries that, "use novel technologies and

diverse biomass feedstocks…" and are invested in with the goal of achieving quantity and quality parity with fossil fuel producers. Some examples of these kinds of biorefineries are listed in Table II.

TABLE II

A SELECTION OF INTEGRATED BIOREFINERIES WITH DETAILS REGARDING THEIR OPERATION [data from DOE, 2017]

Name	**Location**	**Technology**	**Feedstock**	**Product(s)**	**Biofuel Capacity (gal/yr)**
Amyris	Emeryville, CA	Biochemical	Sweet Sorghum	Renewable Hydrocarbons	1,370
Emerald Biofuels	Plaquemine, LA	Thermochemical-HEFA	Corn oil, food processing waste, animal fats, greases	Renewable Hydrocarbons	82 million
POET	Emmetsburg, IA	Biochemical	Corn cobs	Ethanol	20 million
Sapphire	Columbus, NM	Algae	Algae	Renewable Hydrocarbons	1 million

As can be seen from the table compiling data from the Department of Energy, there are many types of biorefineries currently in use. However, most of them adhere to

one of three types of processing. A Biochemical process typically describes an enzymatic system that utilizes microbes for the digestion of starches and celluloses for conversion into usable chemical forms [Kirk-Othmer, 2007]. Thermochemical processes typically involve the breaking down of compounds such as lignin, cellulose, and hemicellulose into their respective chemical compounds using a combination of heat and chemical treatment, typically acid [Kirk-Othmer, 2007]. The final type mentioned above, algal systems, take advantage of the biology of algae to create a multitude of products, ranging from oils to sugars for fermentation [Savaliya, 2013]. Regardless of what is used for processing the biomass, the other observation of note is the varying sources of biomass that are used. All are non-food materials that would otherwise not be disposed of, allowing for more cost-effective production of biofuels in the long run. While all of the above are considered integrated systems, there are no details about the ability to implement them into current biomass processing facilities which would allow for easy transportation and the creation of co-products “in-house” like the refinery described by Fonseca et. al [2014].

C. CARBON FORMS

Carbon is found naturally in two forms, diamond and graphite (Figure 2.2) [McEnaney, 1999].

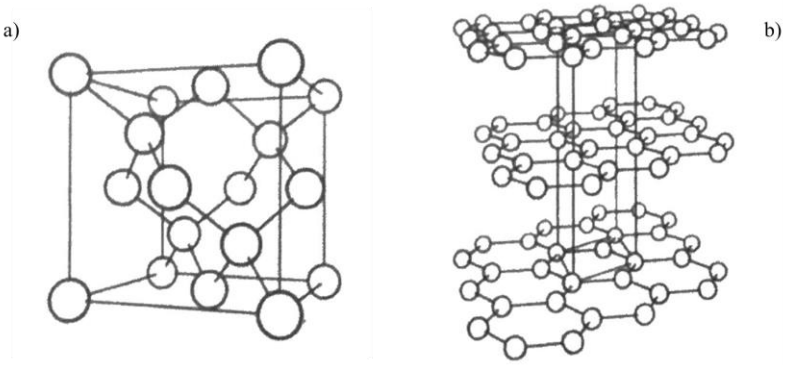

FIGURE 2.2 - Carbon allotropes in the form of a) diamond crystal lattice and b) graphite [Pauling, 1947]

While helpful for cutting, writing, and decoration, these forms are not heavily used in the field of renewable energy. On the other hand, synthetic carbons such as activated carbons and nanotubes are both useful for energy storage purposes. These synthetic types are also easily produced from carbon-rich precursors including plant and animal matter [Pierson, 1993]. Thus, biomass waste streams are a popular option when it comes to activated carbon production. Overall, the majority of synthetic carbons typically fall between amorphous (disorganized) carbons and graphitic (highly organized) carbon. This spectrum of organization allows most carbons to be modified depending on the properties that are required for the various applications in which the carbon will be used [Pandolfo, 2006]. Because most synthetic activated carbons lie in between graphite and amorphous

allotropes in terms of structure, they have characteristics of both the amorphous and graphitic carbon types. This means that activated carbon materials can be both conductive and have a higher porosity that is necessary for many energy storage applications. Most of the carbons used in these various energy applications are formed through heat treatment in an inert atmosphere to allow for carbonization [Pandolfo, 2006; Carrott, 2007]. This process eliminates organic matter and volatile compounds leaving behind a carbon structure that is porous and typically has high surface areas [Pandolfo, 2006].

D. METHODS OF CARBONIZATION AND ACTIVATION

Carbonization and activation have been extensively studied in an attempt to fine-tune the properties of resulting carbons for various applications. Activation, in its most basic form, can best be described as a process that is used to increase the surface area of a carbon source (coal, tar pitch, biomass, etc.). These sources are chosen based on considerations such as price and availability. This increase in surface area correlates to an increase in pore density and distribution. These characteristics can then be taken advantage of in a wide range of applications from filtration to energy storage. Any mechanism that is used to carbonize and activate carbon must therefore eliminate mass within the structure to develop the free spaces that will be taken advantage of in application [Do, 1995].

There are two main activation processes that have been described extensively in carbon research, physical and chemical activation. Physical activation involves the removal of carbon mass and expansion of the physical structure, using gases as a medium

to force the structure to open [Do, 1995]. In most cases, the initial material is either a previously made carbon or the material is first charred in order to create surface variation that the chosen activating gas can permeate [Wang, 2012]. This is then heated to higher temperatures in the presence of the activating gas, typically CO_2 or N_2 where the agent can force its way into the carbon and physically inflate the material. The gases forcing their way through the material creates pores and channels that increase the surface area. Chemical activation, on the other hand, uses activating agents that dehydrate-such as hydroxides, mineral acids, and metal salts-to create the surface area required of activated carbon materials. This method also has inherent benefits due to its mechanism of activation. These include: lower activation temperatures, higher yields, increased pore distribution, a one-step process, and the porosity can be fine-tuned for specific purposes by changing the atmospheric and experimental conditions [Linares-Solano, 2002]. When it comes to choosing which activation agent to use, there are many options to consider. In the case for developing materials for energy storage-which require smaller pore structures-hydroxides are usually used as they have been shown to create narrower pore sizes while maintaining high surface areas [Do, 1995; Lillo-Rodenas, 2003; Wang 2012; Yoon, 2004]. KOH has also been shown to produce narrower pores and requires a lower reaction temperature than NaOH, leading to its use in more studies in order to save energy in large-scale applications of carbonization [Wang, 2012].

The mechanism of hydroxide activation, while used frequently, is still not understood to the extent that many would like due to the complexity of the joint carbonization and activation process. This complexity becomes common-place when using biomass precursors whose physical characteristics can vary from plant to plant, which can result in

a wide distribution depending on the local source of fiber available to producers. A general overview describes that the process begins as a solid-solid reaction and then transitions into a solid-liquid reaction once it is at a high enough temperature [Wang, 2012]. The three main mechanisms proposed to explain the activation reaction are as follows:

1. The carbon structure is etched by the various redox reactions that occur due to the presence of KOH interacting with carbon to form metallic potassium, potassium carbonate, and carbon monoxide. This is generally considered the main instigator of pore formation, the actual "chemical activation" component of the system.
2. A sort of physical activation occurs where water and carbon dioxide formed in the dehydration of the KOH and reduction of potassium carbonate physically expand the pores formed as part of the chemical activation. In this respect, chemical activation is still very much a physical process. However, the assistance of the chemical components to cause actual chemical change to the material in combination with the physical aspects is what allows for the better yields and lower activation temperatures.
3. Metallic potassium formed throughout the process intercalates into the carbon structure as the material becomes plastic at elevated temperatures. This metallic potassium then becomes a part of the final carbon product and is removed when the material is washed (Figure 2.3). At this point in the process, the material has hardened and therefore cannot return to its original shape, leaving the spaces that the potassium deposited in completely open and able to contribute to the overall surface area [Wang, 2012]. This forces the need for an extra processing step when

compared to physical activation; however, it is considerably minimal compared to the benefit of higher yields.

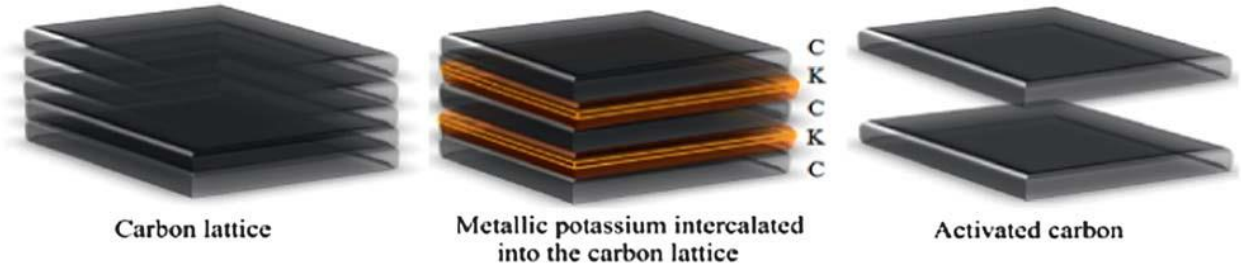

FIGURE 2.3 - Intercalation of KOH into the carbon structure [Wang, 2012]

Ample research has also been performed to show trends of surface areas with change in atmospheric and other experimental conditions [Do, 1995]. As would be expected in a system like this, surface area increases with the addition of more activating agent [Do, 1995]. Other trends that deal more with the fine-tuning of the pore structure (in KOH activation) include temperature, which show that an increase in temperature corresponds to an increase in surface area and micropore volume [Do, 1995]; an important consideration when carbons are ultimately being produced for use in energy storage applications. These factors are all explored when developing an activation process such as the one used in this particular research.

E. ACTIVATED CARBONS FROM BIOMASS IN SUPERCAPACITORS

Supercapacitors are becoming one of the leading devices for electrical energy storage and power due to their rapid storage and release abilities, in addition to their high energy density compared to similar storage devices [Pandolfo, 2006]. Supercapacitors are efficient because of their highly-reversible charge-storage capabilities. This leads to longer cycle-lives and rapid charge and discharge cycles that can provide disbursement of stored energy on demand-an issue with collecting renewably sourced energy directly into the grid [Shukla. 2001]. The primary capacitor type currently under investigation are electrochemical double layer capacitors (EDLCs). Stability, lifespans (up to 500,000 cycles) [Andrieu, 2000], and ease of use have led to the EDLC becoming the most extensively industrialized form of supercapacitors. Its effectiveness compared to standard capacitors comes from the small distance between the electrodes in the device and the increase in charge storage that arises from the surface area of the electrode. Because of this surface area requirement, electrode materials that are stable, have high-surface areas, and are conductive are the best materials to use in EDLCs.

EDLCs work by using the concept of double layer capacitance which was proposed and studied by von Helmholtz in the 19th century [Helmholtz, 1853]. This theory involves the adsorption of charges onto surfaces positioned very close together to store energy in the form of charge separation. This was first used for electrical energy storage by General Electric in 1957 [Becker, 1957] which used carbon electrodes and an ionic liquid as its electrolyte. Later, in 1966, it was recognized that this storage was actually occurring in the double-layer, spurring research into making these capacitors more efficient [Rightmire, 1966]. As described previously, EDLCs are constructed by taking two

electrodes made from a porous material and are separated by an electrolyte and an ion-permeable material that allows for charge to pass through the medium. Because each electrode is considered a capacitor, there are two capacitances taken into consideration making the overall capacitance equivalent to the sum of the two individual capacitances [Andrieu, 2000].

$$\frac{1}{C_{cell}} = \frac{1}{C_1} + \frac{1}{C_2} \tag{2}$$

Each electrode has its own double layer capacitance which can be represented by the following equation;

$$C_{dl} = \frac{\varepsilon A}{4\pi t} \tag{3}$$

Where ε is the dielectric constant, A is the surface area of the electrode, and t is the thickness of the electrical double layer [Shukla, 2000] (Figure 2.4). The above formula shows exactly which aspects researchers need to target when trying to improve device storage capabilities. Increasing surface area of the electrode materials while decreasing the distance between the electrodes leads to higher energy storage potentials. While these can be manipulated fairly easily, there are inherent materials issues that can

build resistivity to charge transfer including resistance between the electrode and the collector, diffusion resistance of ions in small pores, and electrolyte resistance [Burke, 1995]. Therefore, materials that can satisfy the surface area necessities and lower resistivity within the cell are the most promising to use. Activated carbon is one such material due to its relatively high conductivity, high surface area, stability, tunable pore distribution, low cost, and ease of production. Carbons made from biomass present an even better material as they create energy devices from renewable sources instead of coals and anthracites.

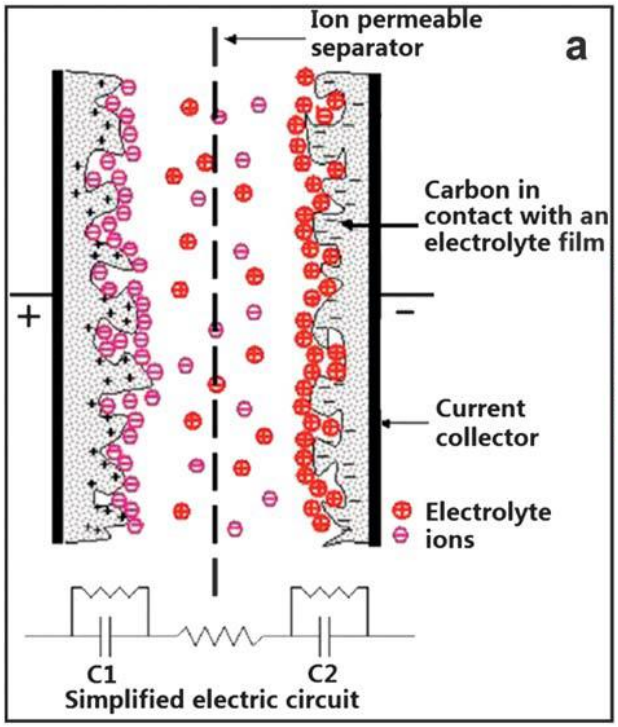

FIGURE 2.4 – Diagram of a standard EDLC [Wang, 2012]

Much research has been performed in attempting to create carbon materials for energy storage from biomass materials. Rice husks have been successfully synthesized into standard activated carbon samples and implemented into supercapacitors with capacitances up to 198.4 F/g [Van, 2013]. Different parts of peanut shells, the inner, lignin-rich layer, and the outer shell have been carbonized and activated separately to create hybrid capacitors that rival current lithium ion devices [Mitlin, 2014]. Tobacco stems have been shown to create effective carbons for energy storage without the need for additional activation chemicals; simple pyrolysis suffices to create the desired material [Beguin, 2015]. Highly graphitic carbon materials with low surface area have been produced from banana peels, allowing for easier charge passage in energy applications [Loftabad, 2014]. Carbon nanosheets with properties similar to graphene have been produced hydrothermally using hemp as the biomass precursor, ushering in a new realm of graphitic material production from biomass [Wang, 2013]. In the majority of the cases presented, the biomass streams in use were typically wastes from biomass processing. However, there were no other steps between waste product and carbon material. From a biorefinery standpoint, there is very little information available of the benefits or detriments to carbon production when the waste fiber is first processed for useful biofuel chemicals.

F. ACTIVATED CARBONS FOR HYDROGEN STORAGE

The United States, along with the rest of the world, is looking for options to transform its energy sector. In order to do this, the Department of Energy has gathered specific

statistics that have allowed for analysis regarding the energy usage of the United States. A 2006 study shows that 20 million barrels of oil are used in the U.S. each day. Two-thirds of this amount is used for transportation alone. Of the total oil used, 55% is currently imported from other nations and is expected to reach 68% by 2025 [DOE, 2006] Therefore, in an attempt to reduce dependence on foreign oil as well as transform the energy sector, oil substitutes are currently being researched to eliminate petroleum completely. Hydrogen has become a strong contender for the transportation sector [DOE, 2005]. Many of the reasons for its popularity as an oil replacement include the ease of manufacture using renewable energy sources including: wind, biomass, hydro, solar, and geothermal. It also contains approximately three times the amount of energy of gasoline, 120 MJ/kg vs. 44 MJ/kg (however, volume based situations show a different story) [Satyapal, 2007]. This in combination with carbon sequestration from current power plants that burn coal allow for a large source of hydrogen that, if combined with the proper infrastructure, could provide large amounts of cost-effective, clean energy for future transportation needs.

These reasons inspired the Department of Energy to establish hydrogen goals for 2015 that included overcoming the following three barriers [Satyapal, 2007].

1. Vehicles running on hydrogen fuel must have a driving range greater than 300 miles (500 km) while meeting all packaging, cost, and performance requirements.
2. Fuel cell system cost must be below $30 per kilowatt while still maintaining durability and performance.

3. Hydrogen production and delivery must be competitive with gasoline and therefore price must fall between $2.00 and $3.00 per gallon of gasoline equivalent.

Another issue that needs to be taken into consideration is whether or not re-fueling would be through reversible on-board storage systems or regenerable off-board storage systems. These systems would influence how hydrogen would be put into the car. In the case of reversible systems, hydrogen could be charged to the vehicle similar to current gasoline mechanisms. Off-board systems would require whatever materials or fuel system is being used to be removed from the vehicle and recharged with hydrogen before being used again [Ahluwalia, 2011; Graetz, 2008].

Many perspectives on how these goals can be met have since arisen. Two options would be to store it as a gas or in its liquid form and have it inserted directly in a tank without any form of storage other than tank itself. Liquid hydrogen, while providing more energy per volume and driving range than its gaseous counterpart, is subject to boil off, leading to cost increases and cycle inefficiencies [Satyapal, 2007]. Since liquefaction also requires a large amount of energy [Zuttel, 2004], compressing the gas and using it in a similar fashion to propane is often the proposed method of non-external material hydrogen use. In order to store it as a gas, pressures of up to 10,000 psi must be used to allow for optimum storage in a cylinder [Utigikar, 2005]. Pressures this high increase the potential mechanical energy extensively and therefore can create a substantial failure in the case of a tank rupture [Stephenson, 2004]. In order to prevent this, specialized tanks would have to be created to support the hydrogen system. These tanks, in an attempt to prevent rupture and hydrogen attack, would most likely be very costly; making it difficult

for the system to keep to the standards set by the DOE. Research is currently being performed on carbon fiber tanks to accomplish this goal, but costs have not been encouraging due to the amount of fiber required to make them safe [Quantum Report, 2005]. In order to make hydrogen a fuel supported by the public, there must be absolute confidence in its safety and utility.

This problem is being deciphered and solved by researching solid materials that can be placed in tanks to adsorb or combine with hydrogen [Satyapal, 2007]. These materials can then allow hydrogen to be stored and used in vehicles at ambient temperatures and pressures, eliminating the need for costly, rigid tanks. The three major categories of storage materials are as follows: metal hydrides, high surface area sorbents/carbon-based materials, and chemical hydrogen storage materials. Metal hydrides, while useful in temperature ranges (25-120 °C) [Sandia, 2005] and pressures (1-10 atm) required for on-board hydrogen storage, have too low of a gravimetric capacity to be effective for long-range driving. Chemical storage requires high pressures and low temperatures in order to release stored hydrogen. For example, ammonia compounds are often named as a possible medium, but the energy required to store hydrogen in the chemical system makes it far too costly [Satyapal, 2007]. Materials that provide the kinetics needed for this kind of hydrogen storage and are relatively easy to produce are activated carbon adsorbents [Satyapal, 2007]. For this work, the focus is on the use of said carbon adsorbents as it allows for fast hydrogen kinetics and lower binding energies than metal hydrides [Satyapal, 2007]. Therefore, there is a lower risk of large temperature increases during charging and discharging, reducing the risk of explosion during fueling. This advantage has also led to experiments binding transition metals to highly-structured

carbons like fullerenes to give the benefit of both the carbon storage and the catalytic assistance from the metal ions. As none of these have been able to effectively create hydrogen powered vehicles, the DOE is still looking for new ideas and opportunities when it comes to hydrogen storage [NAP, 2004].

G. ACTIVATED CARBONS FOR USE IN PEROVSKITE SOLAR CELLS

Metal halides were useful compounds that were being produced as early as 1893 [Wells, 1893]. However, their structure was not fully understood until crystallographic studies were performed on the halides by Christian Moller in 1958 [Moller, 1958]. His studies showed that the metal halides formed a perovskite structure, one that involved two cations differing in size with an anion that had the ability to bond to both (Figure 2.5).

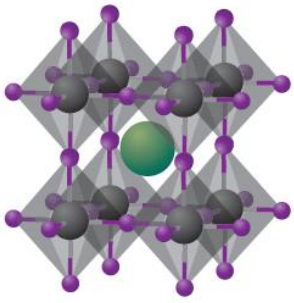

FIGURE 2.5 – Crystal structure of cubic metal halide perovskites [Graetzel, 2014]

In this case, cesium, lead, and a halide were the components of the perovskite studied by Moller. He also noticed that the perovskite metal halide was photoconductive, meaning that it behaved like other semiconductors. Eventually, the cesium was replaced with a more stable and less toxic cation, methylammonium [Weber, 1978]. Due to its astounding optical and electronic properties, the material has been thoroughly investigated in the past couple of decades for its use in solar devices, especially Methylammonium Lead Iodide ($CH_3NH_3PbI_3$). This perovskite is a semiconducting crystal that contains a direct bandgap of 1.55 eV, making it optimal for various photovoltaic devices. This band gap corresponds to an onset absorption of 800 nm, which provides excellent absorption across the entire visible spectrum [Ponseca, 2014]. Weak binding energies of 0.030 eV, small effective masses of electron-hole pairs, and longer carrier-diffusion lengths rivals that of many indirect semiconductors (silicon) of which the most efficient solar cells are currently produced [Mitzi, 2001; Stoumpos, 2013; Xing, 2013; Stranks, 2013]. Once these properties were explored and developed, they were implemented into combination dye-sensitized solar cells, using the perovskite as a sensitizer similar to Ruthenium dyes that were being used at the time. The initial results were disheartening, reaching a minor 3.8% PCE [Kojima, 2009], but one of the main reasons for this was the instability of the crystal in the liquid electrolyte. While structurally sound in dry conditions, perovskites degrade quickly in humidity and liquids [Spiccia, 2015] Eventually, to solve this problem, the liquid electrolyte was replaced with a solid hole transport layer that facilitated the exchange of photo generated electron/hole pairs. The replacement of the liquid electrolyte with this solid layer, called spiro-MeOTAD, doubled previous

efficiencies and also improved stability beyond initial tests. This was the birth of the solid-state mesoscopic solar cell (Figure 2.6).

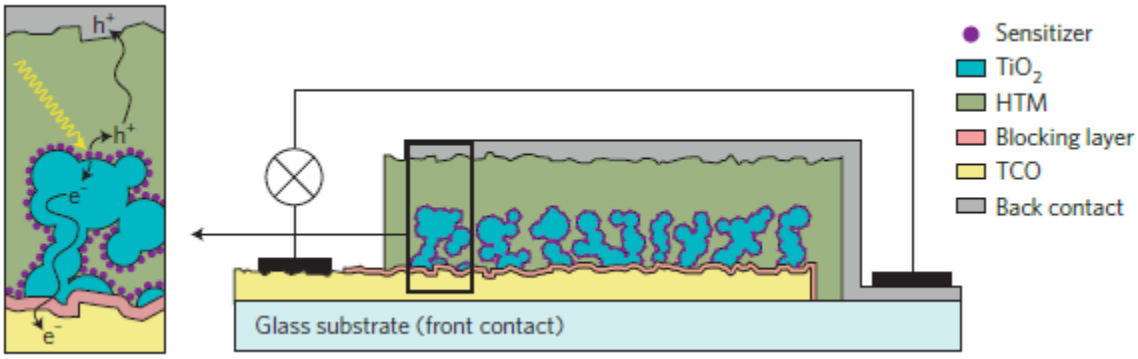

FIGURE 2.6 – Diagram of a mesoscopic perovskite solar cell [Graetzel, 2014]

In these devices, perovskite was deposited on layers of mesoscopic TiO_2 as a way to promote direct electron injection to electrodes made of gold and silver. As time has progressed, so has the design, moving from mesoscopic to planar layers of perovskite and other materials, including carbons for the counter-electrode [Graetzel, 2014; Mei, 2014]. This planar structure allows for simpler processing, reducing costs of an expensive construction. Eventually, layers of material deposited onto glass substrates became the standard for solid-state devices, resulting in efficiencies as high as 12.8% and high stability [Mei, 2014]. Mei et. al also introduced solid-state devices that used a layer of carbon for the counter electrode with perovskite deposited directly into the carbon layer, improving contact (Figure 2.7).

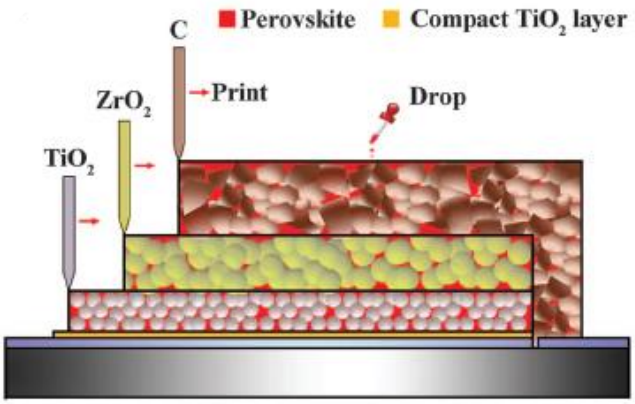

FIGURE 2.7 – Screen printable perovskite solar cell with carbon counter electrode [Mei, 2014]

Before the deposition, the cell layers are screen-printed, allowing for quick, efficient manufacturing. These cells also showed improved stability as the hydrophobic nature of the carbon counter-electrode prevented moisture from damaging the perovskite. While not the most consistent in terms of manufacturing effective cells, carbon layer solid-state devices have exceeded that of dye-sensitized cells while also removing expensive materials from the structural design. Continued research would focus on optimization of electron transport through the device, stability, and continued improvement in materials replacement; thus, lowering the overall cost of manufacturing and operation.

H. OTHER APPLICATIONS OF CARBONS MADE FROM BIOMASS PRECURSORS

While not tested in this work, activated carbons from biomass precursors are used in a variety of pollution control applications not described previously. One of the most

utilized is the use of activated carbons as filtration media for pollutant removal from aqueous and gaseous phases in both industrial and domestic purposes [Dias, 2007; Kirk-Othmer, 2007]. Multiple studies have shown the effectiveness of carbons made from agricultural waste for the removal of color compounds such as Congo red and methylene blue [Karagoz, 2008; Namasivayam, 2002], large compounds that are often used to model pollutants in aqueous environments. Additional studies have investigated the use of these biomass carbons and charcoals on effectively removing actual pollutants that are typically encountered in industry. These include the removal of lead (II) ions with carbons made from gopher spurge (*Euphorbia rigida*) [Gercel, 2007], the removal of phenols with carbons made from sawdust [Hameed, 2008], and the removal of ethyl carbamate-a compound prevalent in alcoholic beverages and soy sauce-using charcoal [Bae, 2009].

The rectification of stack emissions from various industrial plants has led to an investment into carbon capture technologies that often use carbons in their filtration matrix [Mohamed, 2013]. Modified carbons from lignocellulosic biomasses have been investigated to remove sulfur compounds (SOx), nitrogen compounds (NOx), hydrogen sulfide gas, and other volatile organic compounds [Mohamed, 2013]. This has the potential to expand into wide-spread use if industry sees value in producing carbons from the various biomasses that can be found in their area. These would be beneficial not only for their ability to reduce and control pollution, but also potentially utilizing biomass waste streams that otherwise have no purpose.

Activated carbon is also used as a heterogenous catalyst support in aqueous and gaseous systems. As described previously, the mechanical properties of the material

allow for excellent durability in both high temperatures and chemical environments. This, in combination with their porous structure that can support and spread large amounts of catalyst over its surface, creates an ideal interface that allows for increased conversion [Juntgen, 1986]. Wang et.al [2013] demonstrate an effective use of activated carbons from straw to catalyze the esterification of oleic acid with methanol. Knowing this, future research into carbons for the catalysis of biodiesel production could prove to be beneficial for renewable liquid fuels production.

III. EXPERIMENTAL

A. EXPERIMENTAL PLAN

The temperature for carbon activation was set to 950 °C [Do, 1995] to provide the pore size distribution wanted. Carbonization tests were performed to determine the effectiveness of the process and the effect of concentration of activating agent on the resulting surface areas. This was accomplished by varying the concentrations of KOH added to the biomasses in mass ratios of 0:1 KOH to biomass, 0.17:1, 0.17:1 fluffed, and 1:1. All of the fibers used in these tests were post-hydrolysis fibers. Once these results were obtained, the concentration was fixed.

Qualitative fiber was characterized so that differences in the pre and post-hydrolysis fibers could be denoted and to predict the effect of the hydrolysis on surface area. This was performed using SEM imaging. This qualitative imaging could help predict the eventual surface areas of the carbons made as there is a known correlation between precursor surface structure and carbon material surface area. The carbons were then analyzed. The carbons were prepared with both pre and post-hydrolysis DDG fibers and soy hulls and then characterized via BET for surface area and pore sizes, SEM, TEM, and EDAX for structure and chemical composition, and Raman spectroscopy for bond structure and order. All of these values help in determining the physical structure of the material, which could then be compared to literature values and (in the case of BET and Raman) compared to industrial samples.

To see the potential for the carbons in energy storage applications, devices that use carbons effectively were chosen for testing. The first application chosen was use in supercapacitors. In this case, the effect of concentration or surface area was also

investigated. Therefore, the four samples prepared for the concentration tests were used as electrode materials for EDLCs. They were then tested using a voltammeter, providing data on the charge and discharge cycles and capacitance to determine the effectiveness of a supercapacitor. The highest surface area carbons were then used in perovskite solar device applications where solar efficiency determined the effectiveness of the material. Once it was found that they could not work as designed by Mei et. al [2014] due to combustion at high temperatures, they were used as spacers in other parts of the cell and efficiency was measured again. This provided additional insight into the stability of the material. These results led to cleaning experiments using 1 M mineral acids of mono and diprotic varieties to wash the carbons after activation to see if the wash would remove any functional groups that could be impeding performance. Heating tests were then performed to see if the stability at high temperatures improved with the cleaning.

Hydrogen storage was explored next and control carbons were used in dispersal tests on PTFE membranes for a solid-state adsorbent module. Hexane was mixed with differing concentrations of both mineral and sunflower oil to see which solvent combinations created the most effective carbon layers. These oil to hexane ratios were 1:0, 3:1, 1:1, and 1:3. The qualitative results of these tests gave insight into the validity of a solid-state module. Finally, techno economic analysis was performed to determine the monetary value of the carbons made and their potential impact on bioprocessing.

B. MATERIALS

1. Dried Distiller's Grains

Dried Distiller's Grains are leftover materials form ethanol production. In this work, they were obtained from the Brown-Forman Corporation (Louisville, KY) after distillation and drying. They were then prepared as described in the procedures. Composition of the DDG by mass: 32.7% protein, 12% fat, 51.7% neutral detergent fiber, and 2.01% ash.

2. Soy Hulls

Soy hulls were obtained from Owensboro Grain Company (Owensboro, KY). They were used as is for pre-hydrolysis testing or hydrolyzed as described for the DDG for post-hydrolysis testing. No sonication or separation was involved with the soy hulls.

3. MWV Control Carbon

The control carbon was obtained from MeadWestVaco (Richmond, VA). The carbon was wood-derived with a surface area of 1230 m^2/g and an average pore width of 3.620 nm.

4. Potassium Hydroxide

Activating agent in the form of potassium hydroxide was used for all the samples based on literature results. This was obtained from Sigma-Aldrich at 99% purity.

C. EQUIPMENT

DDG was screened through a No. 20 sieve (0.85 mm opening) to separate the fiber-rich and nutrient-rich fractions. The fiber was then soaked in water and sonicated with a

UP200S transonic homogenizer with a 40 mm diameter probe (Hielscher Ultrasonics, Germany). This was then de-watered using a No. 40 mesh screen. Soy hulls were brought in as is and required no additional equipment for pre-treatment. Both biomasses were hydrolyzed in a 6 L percolation reactor with liquid recirculation (M/K Systems Inc, Peabody, MA, Figure 3.1).

FIGURE 3.1 – Percolating reactor used for hydrolysis

Carbons were processed in a MTI GSL-1500X tube furnace with a mullite tube in ceramic boats to create as inert of an environment as possible (Figure 3.2). Pre and post-hydrolysis fibers and carbons were analyzed via SEM using a Vega 3 Tescan (Figure 3.3) and TEM using a Tecnai G2 F30 (Figure 3.4). These provided the imaging and diffraction patterns that helped determine physical characteristics. The Tecnai system was also used for the single-line EDAX run with accompanying software providing the

chemical counts. BET surface analysis was performed using a Micromeritics Tri-Star 3000 (Figure 3.5) which provided the isotherms and surface areas for analysis and comparison. Software used for the analysis was also provided by Tri-Star. Raman Spectroscopy was performed using a Renishaw inVia Raman Microscope and provided Raman spectra that could be used to determine the order of the carbon materials.

FIGURE 3.2 – Tube furnace used to produce the carbon materials

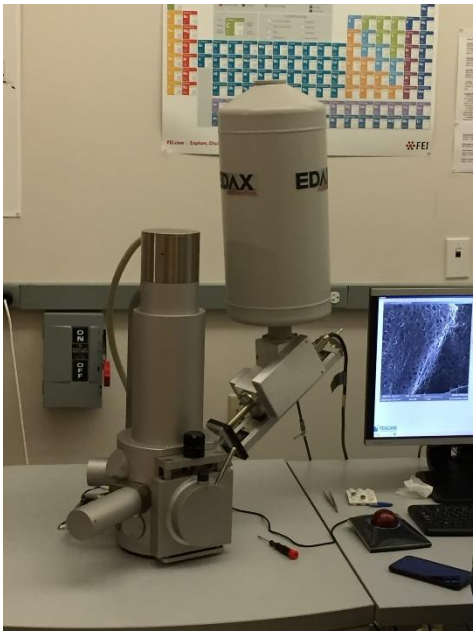

FIGURE 3.3 – SEM microscope used for imaging

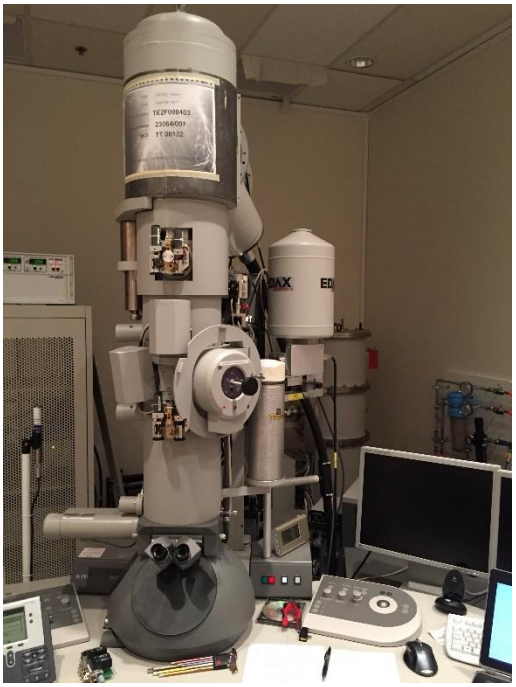

FIGURE 3.4 – TEM microscope used for imaging and EDAX analysis

FIGURE 3.5 – BET surface analyzer used for surface area and pore size analysis

Supercapacitor testing required the use of an Arbin Instruments Supercapacitor Testing System (Figure 3.6) to perform cyclic voltammetry. Accompanying software provided the user interface to obtain the data. Current–voltage characteristics of the carbon devices were measured with a solar simulator composed of light source and a digital source meter (Keithley Model 2400). The light source was a 450 W xenon lamp (Oriel) equipped with a Schott K113 Tempax sunlight filter (Praezisions Glas & Optik GmbH) to match the emission spectrum of the lamp to the AM 1.5G standard. Before each measurement, the light intensity was calibrated by a Si reference diode equipped with an infrared cut-off filter (KG-3, Schott). All measurements were conducted using a nonreflective metal aperture of 0.16 cm^2 to define the active area of the device and avoid light scattering through the sides.

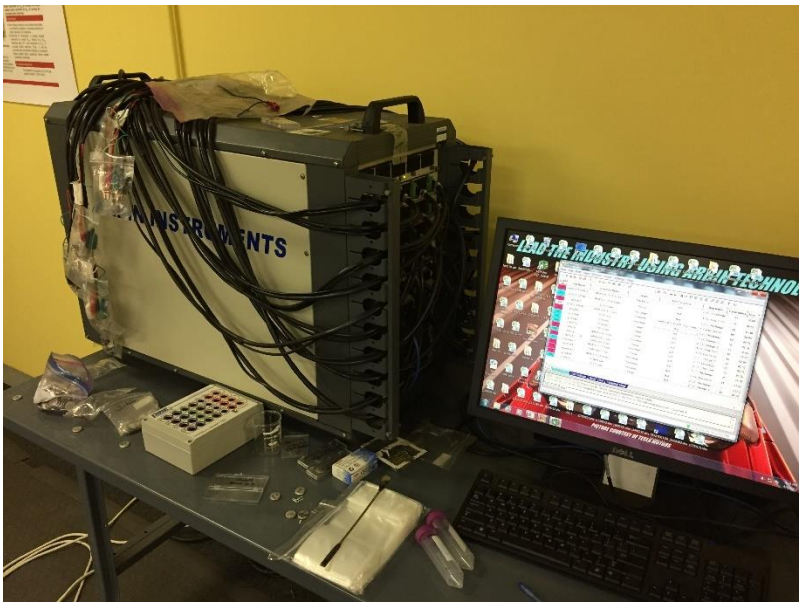

FIGURE 3.6 – Supercapacitor testing system used for cyclic voltammetry to measure supercapacitor qualities

D. EXPERIMENTAL PROCEDURE

1. SEPARATION AND CLEANING OF THE BIOMASS FRACTION

The first step was to prepare the biomass for potential hydrolysis via the separation of the fiber-rich and nutrient-rich fraction. This was first described for DDG by Lupitskyy et. al (2014). When treated in this manner, the fiber-rich fraction was kept for hydrolysis due to higher levels of hemicellulose in the material. This fraction was then treated in one of two ways depending on the need.

i. Pre-hydrolysis samples: Distillers grains were screened using a No. 20 (0.85mm opening) sieve. The coarse fraction from the screening was used for hydrolysis purposes. The coarse fiber was then mixed with 1 L of water and sonicated for 30 minutes at 200 W

power using a transonic homogenizer with a 40 mm diameter probe. It was then dewatered using a 40 mesh screen.

ii. Post hydrolysis samples: After drying, the de-watered DDG fibers were hydrolyzed in a 6 L percolation reactor with liquid recirculation (M/K Systems Inc, Peabody, MA). The samples used in this work were hydrolyzed at 120 ˚C using 0.4% sulfuric acid concentration. The remaining residual fiber was then dried in an oven at 110 ˚C until.

2. ACTIVATING AGENT IMPREGNATION

The second step was to mix the precursor material and the activating agent. In most studies involving the production of activated carbon materials, solid activating agent was added directly to the precursor stream as a mixture. To ensure even distribution of the activating agent, the required mass of KOH was dissolved in solution and then mixed and dried as described below. Five grams each of soy and corn fibers from pre-hydrolysis as well as post-hydrolysis were mixed with a KOH solution consisting of desired concentration of KOH and 15 mL of deionized water. For example, 5 g of KOH in solution would yield a 1:1 ratio with 5 g of grains. They were then mixed using a vortex mixer until they formed a thick paste. This paste was then allowed to dry at 80˚C.

3. CARBONIZATION

The dried, impregnated samples were placed in a ceramic boat placed in the center of a tube furnace. This was then sealed with end caps that contained hoses to allow for the utilization of an ultra-pure nitrogen blanket. The tube was pressurized to 10 kPa above atmospheric pressure and the furnace was started. The programmed ramp rate was

10˚C/minute until 500˚C and then was increased to 20˚C/minute up to the final temperature of 950˚C where it held for one hour. The sample was then allowed to cool naturally under the Nitrogen blanket before removing it from the furnace. The samples were washed thoroughly with deionized water in a paper filter and air dried.

4. SURFACE AREA ANALYSIS AND MATERIAL CHARACTERIZATION

The samples were analyzed using a BET surface area analyzer using nitrogen gas as the adsorbed gas at 77.3 K. The samples were degassed before the analysis at 160˚C for two and a half hours, then placed in the machine which submerged the tubes with the samples in liquid nitrogen. Samples were imaged with a Scanning Electron Microscope (SEM) to show the differentiation in pore size, fiber structure, and surface defects for both post and pre-hydrolysis biomass and carbon samples. Transmission Electron Microscopy (TEM) with a combination of a single line EDAX analysis was performed to look at graphitization and composition of the sample. Raman spectroscopy was performed to determine spectra of each sample.

5. SUPERCAPACITOR PREPARATION AND MEASUREMENTS

Electrochemical measurements were conducted for the use of ACs in a supercapacitor structure (EDLC). For this, the electrodes were prepared using the various surface area ACs prepared after activation with varying ratios of KOH. The electrode materials for both the cathode and anode were prepared using 90 wt% active material (ACs) with 2 wt% AB (acetylene black) and 8% PVDF (Polyvinylidene fluoride) binder distributed in NMP (N-Methyl-2-pyrrolidone) solvent. The well-mixed slurry was coated

onto an aluminum foil using the doctor blade method. The electrodes were then dried at 180 ˚C for 3 hours under vacuum. These were transferred to a glove box and a standard 2032 configuration coin cell was then constructed with the electrodes. The separating layer was asbestos and the electrolyte was 1.5 M TEAPF6-PC (Tetraethylammonium hexafluorophosphate in propylene carbonate) solution. Cyclic voltammetry was then performed using a supercapacitor testing system. Charge and discharge cycling was conducted for 1000 cycles between 0 and 3.5 V at a current density of 500 mA/g. The data was then graphed and used for calculations as described in the results and discussion section.

6. PEROVSKITE SOLAR DEVICES

a. Paste Preparation

Titanium Oxide and Zirconium Oxide pastes were prepared as described by Graetzel et. al [Graetzel, 2007]. 6 grams of TiO_2 powder was mixed with 1 mL of acetic acid and ground in a mortar for 5 minutes. 5 x 1 mL portions of water were added to the paste and ground for 1 minute each before the next portion was added. 15 x 1 mL portions of ethanol were added to the paste and ground for one minute before the next portion was added. 6 x 2.5 mL portions of ethanol were added and ground for 1 minute before the next portion was added. This paste was transferred to a beaker with 100 mL ethanol and stirred for 1 minute on a stir plate. The solution was then sonicated with an ultrasonic horn (2 seconds work + 2 seconds rest) 30 times and stirred again for another minute. 20 grams of terpineol was then added to the solution. This solution was then stirred with a magnetic tip for 1 minute and sonicated in the same manner as before. It was then stirred

again for an additional minute. 30 grams of 10% ethyl cellulose solution in ethanol was added to the solution. The solution was stirred for 1 minute, sonicated as previously described, and stirred for an additional minute. This entire stir/sonicate/stir procedure was then repeated two times making the solution go through the previous stir/sonicate/stir method a total of three times. The ethanol was then evaporated using a rotary evaporator and ground in a three roll miller. This procedure was also done with both ZrO, standard carbon, and the biorefinery carbons produced. ZrO paste was also made with 10 wt.% biorefinery carbon.

b. Device Preparation and Testing

Standard-Perovskite solar devices were manufactured in the manner described in Mei et. al [Mei, 2014]. Clean FTO (Fluorine-doped tin oxide) glass was used as the substrate. The glass was placed on a hot plate and sprayed with suspended TiO_2 nanoparticles and sintered at 450 °C for 15 minutes. The glass was removed from the hot plate and allowed to cool. The glass was then screen printed with TiO_2 paste, sintered at 450 °C for 30 minutes, cooled, and then screen printed with ZrO paste. The cell was sintered again at 450 °C for 30 minutes and the carbon paste was screen printed onto the cell. This was then sintered at 450 °C and transferred to a case when cooled. Once cooled, perovskite was deposited onto the carbon layer via drop-casting and then put in a desiccator to dry. Once dry, contacts were applied to the glass and the cell's performance was measured using a standard 1.5 AM, 1 sun lamp.

c. Zirconium Layer Exfoliation

Devices were made with the 10% carbon-infused ZrO to see if the sintering process in combination with the volatility of the biomass carbons could increase the ZrO surface area and there increase the conductivity of the overall device. These cells were manufactured and tested in the same manner as described previously.

d. Effects of Washing with Inorganic Acids on Carbon Sintering

Biorefinery carbons were washed in 1 molar solutions of HCl, H_2SO_4, and HNO_3 by stirring the carbon material in them for approximately 30 minutes. The acids were then disposed of and the carbons were washed two more times with clean DI water. They were then oven dried at 90 °C until completely dry. Carbon pastes were made from the varying carbons as described previously and they were doctor bladed onto clean FTO glass, using Scotch tape as a boundary. They were then sintered on a hot plate at 350 °C in air for 30 minutes. The masses of the clean glass and the glass with the carbon layer were measured before and after sintering. The relative weight loss was then calculated and compared to the weight loss of a paste made from uncleaned carbons.

7. CARBON LAYER FORMATION FOR HYDROGEN STORAGE MODULES

The biorefinery carbons were tested for effective deposition onto a membrane for hydrogen storage module production. MWV control carbons were mixed in varying combinations and ratios of solvents and binders and run through a vacuum funnel through a PTFE membrane to deposit a layer of carbon on the surface. This carbon suspension

was always 2% carbon by mass, but the masses of the solvents and binders varied. Initially, solvents including ethanol, isopropanol, and toluene were used as they could allow for evaporation of the solvent and thus not inhibit the pores for hydrogen storage. Once it was found that solvents alone would not work, different types of oils were used in differing ratios with solvents to form a binding solution that would also disperse the carbons evenly. The ratios tested were 1:0, 1:1, 3:1, and 1:3 ratios of mineral oil to hexane and the same ratios of sunflower oil to hexane. The differing viscosities allowed for process comparison. They were then qualitatively analyzed for their ability to form an even layer that settled appropriately on the membrane.

8. TECHNOECONOMIC ANALYSIS

The effect of carbon production on industrial bioprocessing was considered by analyzing costs of materials and energy into carbon production in addition to profits made from selling the carbons at market prices. DDG amounts were varied to see the effect of throughput on profit. Prices for materials were compiled using the Louisville Water Company, Alibaba, and the USDA as references. Energy prices were based on industrial values for the Louisville area. Total residual fiber into the system for carbon production alone ends up being approximately 1/5 of the total input as the fiber rich fraction is approximately 35% of the material, and approximately 40% of that fiber is removed in the form of xylose during the hydrolysis process. Parameters for operation included temperatures and pressures as described in the carbonization procedure, 350 operating days at 22 hours per day, and three shifts with one operator each at $100,000 per operator per year for salary and benefits. Initial capital equipment cost was not

included in these calculations. Additional parameters including the individual prices of the materials, heat capacities used, and calculations performed can be found in Appendix A. Some special considerations include the use of the self-sustaining pyrolysis temperature. When it comes to biomass pyrolysis, there is a specific temperature at which the exothermic nature of the reaction is able to sustain the heating of the material to that temperature. 600 °C is the lower end of a range described by Idris et. al [2016] for the maximum self-sustaining pyrolysis temperature. Therefore, energy calculations were based on the heat input required to heat the volume of nitrogen in the system above the 600 °C mark and the initial start-up for 10 tonnes of material. Recovery of materials such as the nitrogen gas and pyrolysis oil were considered. The pyrolysis oil was assumed to heat the dryers necessary for the processing.

IV. RESULTS AND DISCUSSION

A. GENERAL DISCUSSION AND OVERVIEW

Up until this point, biomasses from a variety of resources have been used to create activated carbons, but never in the context of a biorefinery operation. Creating value-added co-products from a biorefinery makes an integrated system that is both sustainable and profitable for the parent company. Therefore, the experiments here were completed not only to create a useful energy storage product from sustainable resources, but also to denote the effects of biorefinery processes on the creation of that co-product. Literature indicates that residual biomasses are typically converted to activated carbon materials directly if they are indeed taken advantage of in this manner. On the other hand, biofuels manufacturers producing ethanol and plant sugar streams typically burn their residual biomass streams for process heat or sell them back to farmers for animal feed. There is no indication in the literature that these processes have been combined previously to create an integrated bio-refinery that could further environmentally-conscious production of energy storage materials while improving biorefinery economics. Producing carbons with this material can give insight into the effect of hydrolysis and other biofuel treatments on the precursor material and its carbon-production potential. This information can then be used to assess different biomasses for their integrated bio-refinery potential.

A diagram delineating the conversion of biomass waste streams to carbons is presented in Figure 4.1. The simple flow diagrams compare the processing as is typically done in industry currently to that of an integrated biorefinery.

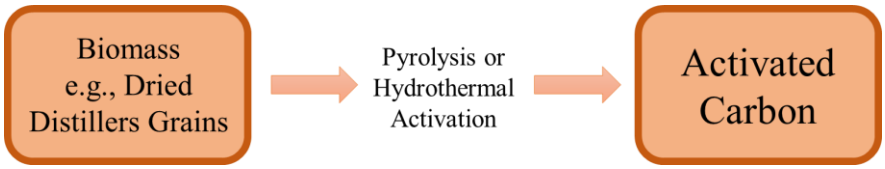

(a)

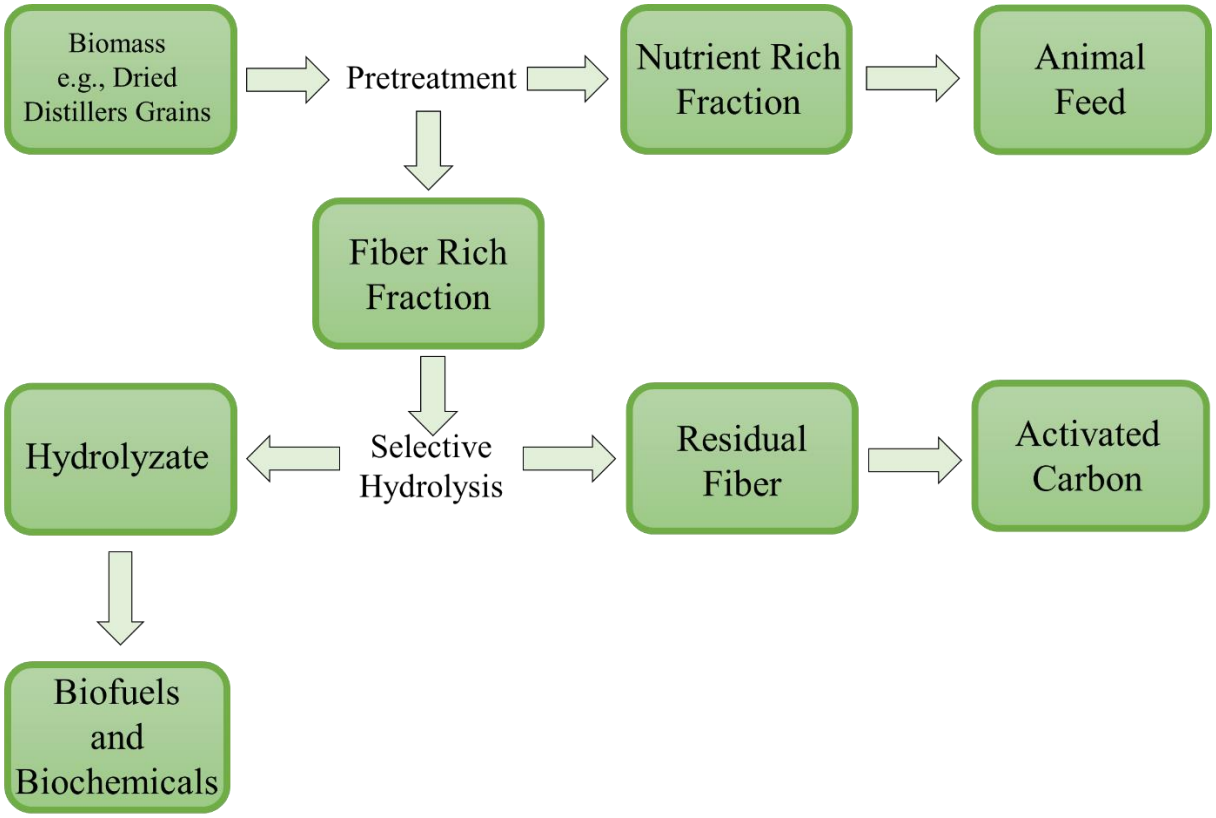

(b)

FIGURE 4.1 - A comparison of standard process steps in the (a) direct conversion of biomass to high surface area carbon as compared to (b) conversion to activated carbon as part of a C5 integrated biorefinery process.

The benefits of this integrated system can result in a plethora of different products and sources of revenue, in addition to the biofuels produced. The only limit to the variety of products is the type of biomass used. Figure 4.1 (b) presents a C5 refinery using DDG,

however, this integrated refinery concept for the creation of multiple co-products could be applied to any biomass that is available. One simply must decide which products they would like to produce from the biomass available to them. This makes the concept transferrable to any geographic location and therefore applicable in many different agricultural processing plants. In the case presented here, the value-added co-products are meant to assist with costs associated with bioethanol production and beverage alcohol distillation by creating revenue streams from animal feed, activated carbon, and biofuels. The focus of this thesis looks at the production of the activated carbons, the characterization of the fibers pre and post-activation, the use of these carbons in energy storage applications, and their potential revenue based on material balances, energy balances, and equipment costs.

B. MATERIAL CHARACTERIZATION

1. Fiber Characterization

Fonseca et. al [2014] described the effects of hydrolysis on DDG fibers in their discussion of the C-5 biorefinery concept. In this work, to corroborate as well as explore hydrolysis effects on materials other than DDG, SEM imaging of the biomass fibers both pre and post-hydrolysis was performed to show the qualitative differences between pre and post-hydrolysis fibers for both DDG and soy. These images are shown in Figure 4.2

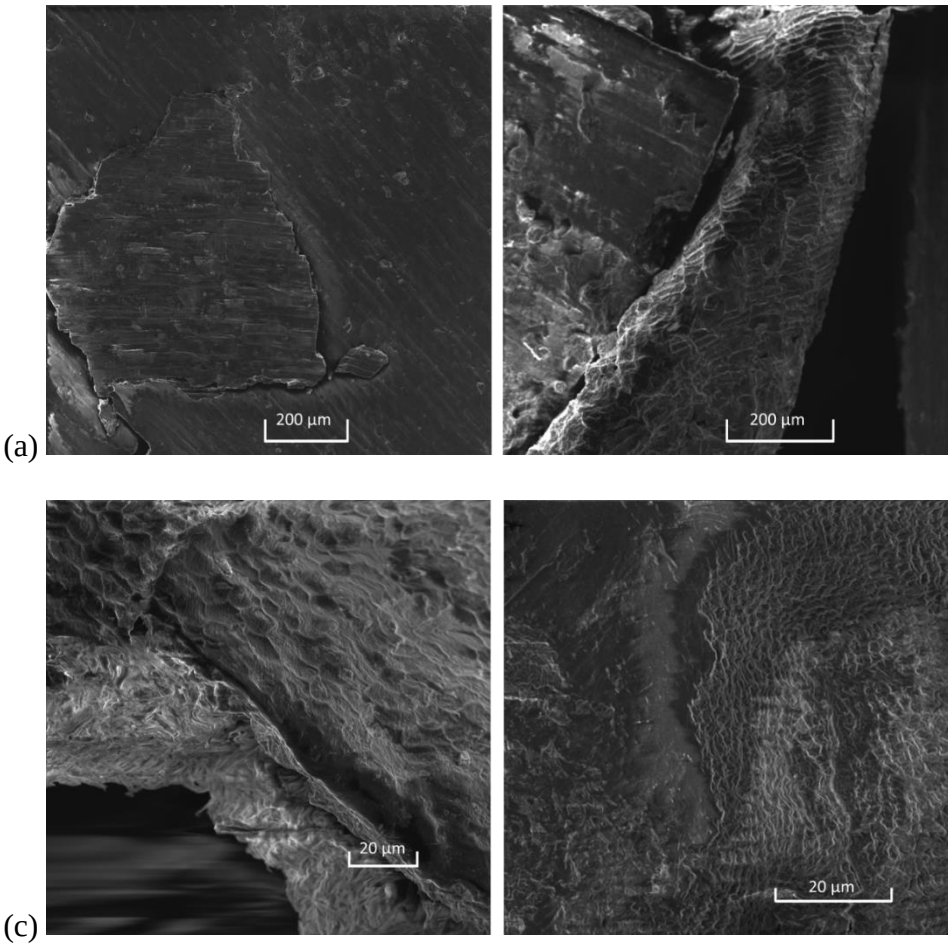

FIGURE 4.2 - SEM images showing differences in surface structure between (a) pre and (b) post-hydrolysis DDG fibers and (c) pre and (d) post-hydrolysis soy hulls.

In the case of both the DDG and the soy, there are dramatic differences in surface morphology. The pre-hydrolysis fibers (Figure 4.2 a and c) both show relatively flat, smooth surfaces with the DDG looking like pressed sheets of paper and the soy forming an amorphous, fluid structure. The post-hydrolysis fibers for both biomass types showed an increased surface structure. This surface structure can best be described in both the DDG and the soy as a dehydrated form of the initial fiber. The fiber appears to shrivel and gain texture along cell boundaries as denoted by the organized ridges in the images. This is due to the acid activation during the hydrolysis process and removal of the

hemicellulose and other structural compounds from the original fiber. This increase in surface texture allowed us to predict, based on literature analysis, that the carbons made from post-hydrolysis fibers would have higher surface areas than the carbons made from the pre-hydrolysis fibers.

2. BET Theory

To accurately measure the surface areas of different solids, the Brunauer-Emmett-Teller theory has become the standard for technical instruments to do so. While BET is the most utilized theory by technical instruments, it is originally derived from the Langmuir surface theory. Solids have a lattice structure, like any crystal, and therefore have definite spaces to which gases can adsorb [Langmuir, 1918]. Langmuir surface area is then based on the adsorption of atoms on the surfaces of solids. The model is kinetically derived, using the rates of adsorption and desorption for each individual space on the surface. A fraction of the rates can then be derived, allowing for prediction of the fraction of spaces covered at differing concentrations. This is directly related to pressure as the system is assumed to be ideal. To measure surface area, the volume of gas adsorbed at different relative pressures can be used along with the contact angle of the adsorbed gas to estimate a surface area. In the case of Langmuir surface areas, this only considers the volume necessary to form a monolayer on the solid. In the case of BET surface area, the model allows for adsorption to occur beyond the simple monolayer [Brunauer, 1938], taking into consideration the fact that adsorption occurs in multiple layers with gas molecules building on each other. Thus, BET surface area would be more accurate for surfaces on which multi-layer adsorption occurs. However, it should be

noted that solids such as activated carbons can have advanced adsorption due to micropores. This indicates that BET surface areas could be an overestimation, but are still included in this work for comparative purposes [Rouquerol, 2007]. Equation 5-1 presents the BET equation as derived by Brunauer, Emmett, and Teller.

$$\frac{1}{v[\left(\frac{Po}{P}\right)-1]} = \frac{c-1}{v_m c}\left(\frac{P}{Po}\right) + \frac{1}{v_m c} \tag{4}$$

In Equation 4, P is the equilibrium pressure, Po is the saturation pressure of the gas at that specific temperature (77 K in the case of Nitrogen), v_m is the volume of the monolayer, and c is described in Equation 5.

$$c = \exp(\frac{E_1 - E_L}{RT}) \tag{5}$$

In the formula for the constant, E_1 is the heat of adsorption for the first layer, and E_L represents the heats of adsorption for the subsequent layers that deposit on top of the first. This can be re-arranged to yield isotherms that can indicate the porosity of materials based on the shapes of the curves. Surface area analyzers work by analyzing the amount of gas that is required to reach specific equilibrium pressure points along a spectrum from

P/Po=0 to P/Po=1, or the saturation pressure. The machine, knowing the volume that is required to reach those equilibrium pressures, can then plot the volume adsorbed at those pressures, and theories regarding the isotherm shape can then be applied to the resulting data. From these isotherms, empirical models can fit the data and provide surface areas of the solid. This is done by an integration of the surface knowing the volume of gas added and the mass of the material in the system.

3. *Activating Agent Studies*

KOH activation is a complex process that involves multiple reactions taking place within and on the surface of the biomass structure. The process also involves characteristics of physical activation which including the expansion of the material via gas release during heating. This results in three main explanations for change in the structure of the material [Lillo-Rodenas, 2003]. Surface area increases due to etching of the surface by the various redox reactions that occur between the potassium compounds and the increasingly free oxygen atoms available in the fiber structure. Water vapor and carbon dioxide result from surface reactions and decomposition of material at high temperatures. These vapors increase the pore volume and develop the porosity in a form of physical activation. Finally, the material is expanded due to metallic potassium layering itself into the structure of the fiber and then is removed during the washing process. The resulting material is a less dense, expanded carbon structure with a higher surface area that is dependent mainly on the physical structure of the precursor [Lillo-Rodenas, 2003].

To determine appropriate concentrations of KOH to use in the experiments, preliminary work was performed with DDG residual fiber to give a data profile that demonstrated the effect of concentration of KOH and fluffing of fibers on both surface area and pore size. Samples were fluffed to aerate and ensure maximum surface area. Four samples were treated and carbonized in the manner described in the procedures at KOH to fiber mass ratios of 0:1 (S1), 0.17:1 (S2), 0.17:1 – fluffed (S3), and 1:1 (S4). As expected and described in the literature [Frackowiak, 2001], surface area and pore volume increased with increased KOH concentration (Table III), while pore distribution skewed toward the micropore range with increasing KOH concentration as indicated by the micropore volume increase. The non-activated sample shows little to no adsorption in any range, representing an almost complete absence of pores. The two carbons activated with 0.17:1 mass ratio of KOH both show curves typical of a material with exposed micropores where the majority surface area is within those pores. The 1:1 mass ratio of KOH yields a curve typical of carbons with mainly mesopores with microporous regions in the 1.5-10 nm range [Frackowiak, 2001]. These values are supported by the shape of the isotherms presented in Figure 4.3. The isotherms for the control and 0.17:1 ratio carbons are mainly linear, showing monolayer development across the entire pressure spectrum. This indicates that there is little internal volume; the majority is external. On the other hand, the 1:1 sample shows the standard shape of a Type II and Type IV isotherm (IUPAC) which indicates a mesoporous/microporous structure, ideal for energy storage devices.

TABLE III

IMPACT OF KOH CONCENTRATION ON PORE SIZE AND BET SURFACE AREA

	Average Pore Width (nm)	BET Surface Area (m^2/g)	t-Plot Micropore Volume (cm^3/g)
Control DDG – S1	8.39	0.47	0.0004
0.17:1 KOH to DDG – S2	2.11	774.34	0.342
0.17:1 KOH to DDG Blended – S3	2.08	744.07	0.329
1:1 Mass Ratio KOH to DDG – S4	2.92	1705.575	0.233

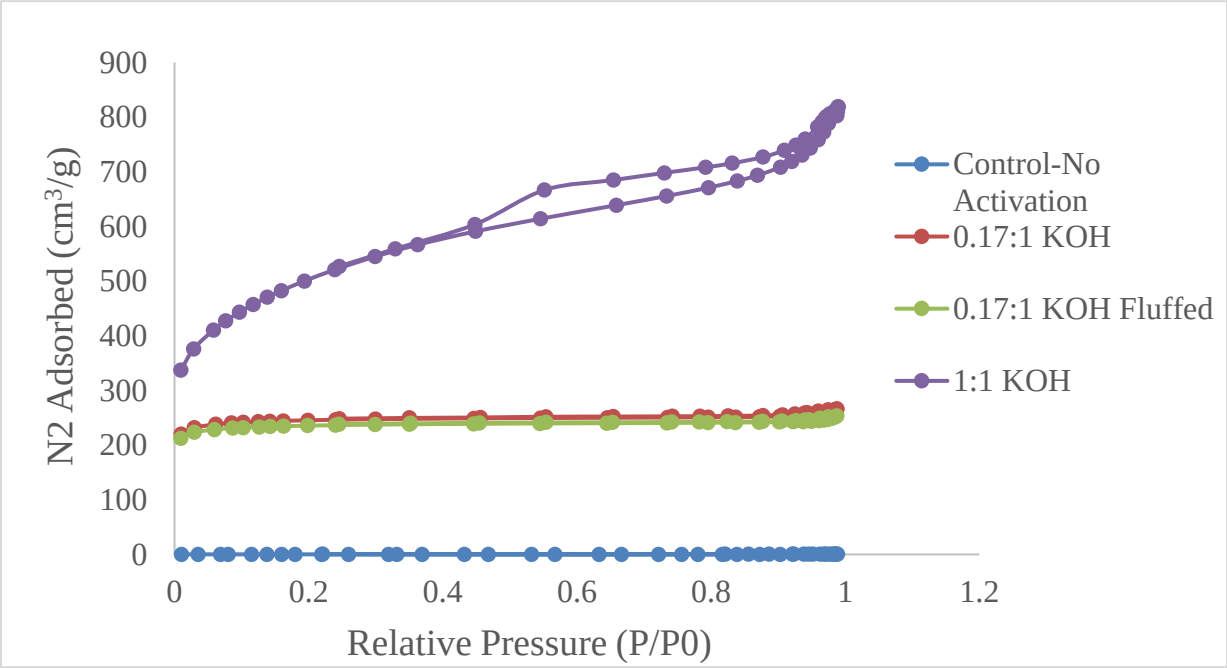

FIGURE 4.3 - Adsorption isotherms from KOH activated carbon samples showing the effect of activation agent concentration on Nitrogen uptake at 77 K

Once an optimum KOH to biomass ratio was found, the experiments were repeated on both pre and post-hydrolysis fibers.

4. Surface Area Comparisons of Carbons form Pre and Post-Hydrolysis Biomasses

The surface areas of activated carbons produced from pre and post hydrolysis fibers are compared in Table 5-2. The corresponding isotherms are given in Figure 5-4. KOH to fiber ratio of 1:1 was used as the activation recipe.

TABLE IV

SURFACE AREA AND PORE WIDTH DATA COMPARING CARBONS MADE FROM PRE AND POST-HYDROLYSIS DDG FIBERS AND SOY HULLS AND CONTROL CARBON MADE FROM WOOD (MWV)

Sample (1:1 KOH to Grains)	**BET Surface Area (m^2/g)**	**Average Pore Width (nm)**	**t-Plot Micropore Volume (cm^3/g)**
DDG: Pre-Hydrolysis	10.44	9.533	n/a
DDG: Post-Hydrolysis	1705.58	2.922	0.233
Soy: Pre-Hydrolysis	689.03	2.652	0.213
Soy: Post-Hydrolysis	1316.34	2.202	0.392
Control: MWV	1226.71	3.620	0.217

Pre-hydrolysis fibers were carbonized with KOH mixture, hydrolyzed fibers were run as described in the experimental section before being carbonized, and the control sample comes from an industrial activation process.

As shown in Table IV, the surface areas of carbonized fibers from pre-hydrolysis DDG and soy were drastically different. The AC from pre-hydrolysis DDG is only 10 m^2/g compared to 689 m^2/g for soy. However, the surface area of AC from post-hydrolysis DDG increased dramatically to about 1700 m^2/g compared to a moderate value of about 1300 m^2/g for post-hydrolysis soy. This discrepancy is most likely due to the less dramatic change in surface structures of the soy after it goes through the hydrolysis process (Figure 4.2). The pre-hydrolysis soy already has an intricate and defined surface structure, which explains the relatively high surface area of 600 m^2/g after carbonization. The change in surface structure of soy seems to only provide enough surface change to achieve 1300 m^2/g post hydrolysis carbons.

The corn fiber presents a very different surface structure. Corn fiber in its natural state has a tough protective layer that is selectively hydrophobic. As shown in Figure 4.2 (a), this provides a smooth structure made up of small, rectangular, interlocking units that provide a barrier from outside elements in nature [Campbell, 2013]. This can prevent development of surface area and, therefore, prevent production of higher surface area carbons if the fiber alone is used as a precursor. Figure 4.2 (b) is an image of post-hydrolysis fiber showing a highly etched surface. The pericarp, being removed, leaves behind cellular block structures with obvious depth. This provides a very small surface area of .7844 m^2/g but high potential to increase due to its jagged surface. The soy fibers present pentagonal cells that form a honeycomb-like structure. This structure and the observed lack of an outer protective coating like the DDG would explain the larger surface area value for carbonized, pre-hydrolysis soy compared to the DDG.

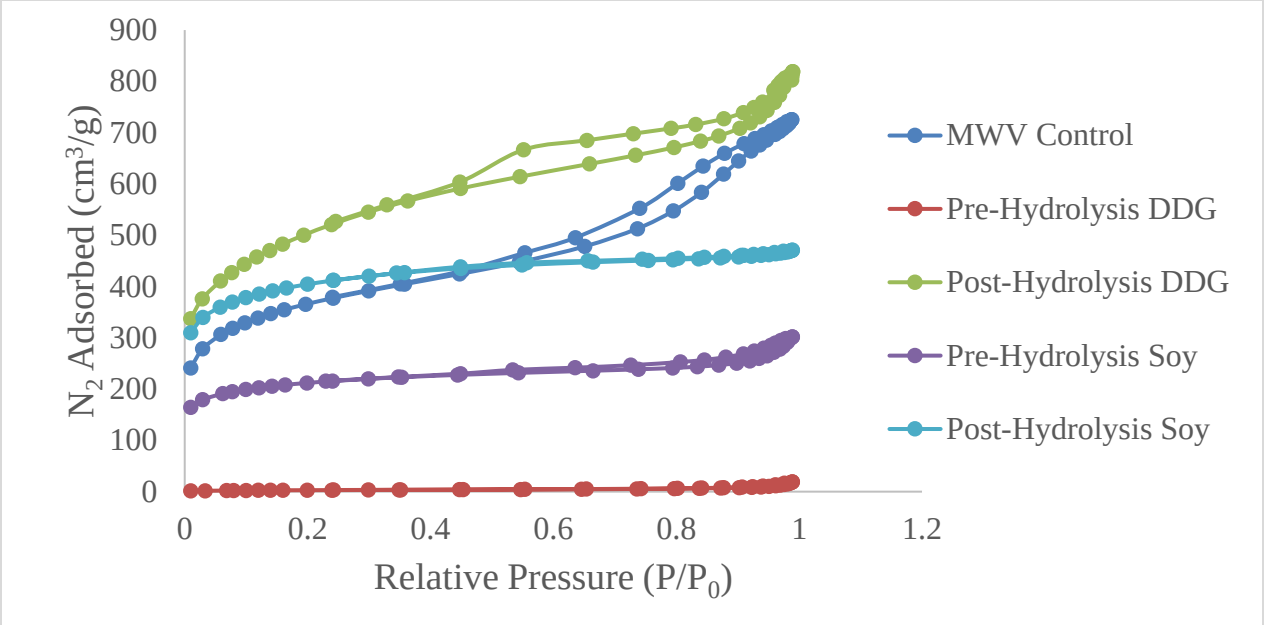

FIGURE 4.4 - Adsorption isotherms comparing quantity of Nitrogen adsorbed with each carbon sample to the relative pressure at 77 K

The isotherms in Figure 4.4 follow noticeable increases in the slopes of the beginning of the isotherms as the relative pressure increases. In the case of the materials with higher overall surface areas, the isotherms would follow Type II and Type IV isotherms denoted by IUPAC [Thommes, 2015]. This curve is defined as an S-curve with increase in the initial range of the relative pressure indicating the presence of micropores. This is prevalent in the post-hydrolysis DDG, post-hydrolysis soy, and the MWV control. This initial slope is followed by a relatively flat portion that is indicative of the formation of the monolayer with a final increase as the equilibrium pressure approaches the saturated pressure. This increase is associated with the onset of multi-layer adsorption. The hysteresis loop that is present for the DDG and MWV sample indicates capillary condensation, indicating a variety of mesopores that cause the nitrogen gas to condense into a liquid state due to the constriction of the molecules and the saturation of the gas.

The lack of hysteresis in the soy could indicate that the surface area described by it is either completely microporous or external. These isotherms predict that both the DDG and soy carbons could be used effectively in energy storage devices, but the soy would perhaps be more useful as a conductive material whereas the DDG could be more effective at physically storing charge.

As demonstrated by the data, there was a dramatic increase in the surface area of the carbons produced from pre and post-hydrolysis fibers. This is expected knowing that the chemical activation process is dependent on the surface structure of the precursor. The fibers that had variant and fibrous surface defects provided a good medium for KOH to react with the surface. Both residual fibers from DDG and soy were able to produce carbons that exceeded 1000 m^2/g in terms of surface area as well as maintained an average pore size of around 2 nm. This shows that both could be used as a viable fiber starting material for AC. More importantly, it opens the door for a wider variety of agricultural biomasses to be implemented in activated carbon production. By pre-processing the fibers, etching the surface while gaining a valuable co-product in xylose, biomasses similar to corn and soy that are unable to produce high surface area carbons without modification can now be used to create an additional, highly valuable co-product that would otherwise not be possible.

5. TEM Studies

In order to explore the physical and chemical structure of the activated carbons, transmission electron microscopy (TEM), and Raman techniques were used to look at the arrangement of the carbon and the types of bonds between the carbons. TEM imaging

(Figure 4.5) and corresponding diffraction patterns (Figure 4.6) for carbons derived from pre and post-hydrolysis samples are typical of carbon materials. Figure 4.5 shows variations in plate structures between the pre and post-hydrolysis DDG and soy.

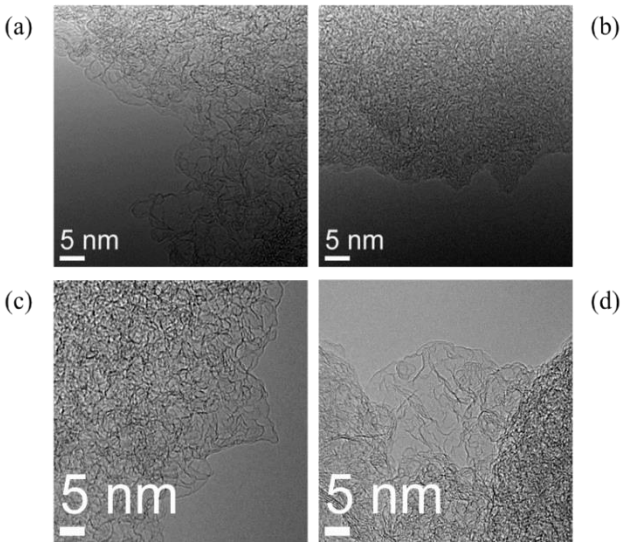

FIGURE 4.5 - TEM images showing organization of the carbon structures on the nano-scale. (a) Carbon from pre-hydrolysis DDG fiber, (b) carbon from post-hydrolysis DDG fiber, (c) carbon from pre-hydrolysis soy hulls, (d) carbon from post-hydrolysis soy hulls

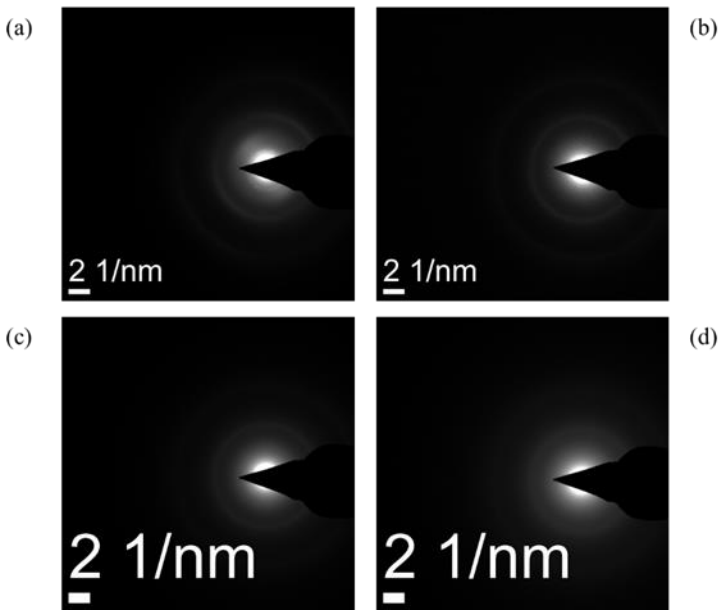

FIGURE 4.6 - Diffraction patterns of the carbon samples. (a) Carbon from pre-hydrolysis DDG fiber, (b) carbon from post-hydrolysis DDG fiber, (c) carbon from pre-hydrolysis soy hulls, (d) carbon from post-hydrolysis soy hulls

Both of the pre-hydrolysis samples (Figure 4.5 a and c) show similar graphitic planes, as seen toward the edges of the image subject. Both contain larger crystalline sections and very little organization in the main sheets of the material. Both also showed two circles radiating from the material source (as shown in Figure 4.6 a and c) – a pattern expected for carbon materials. The soy, however, show a little more exfoliation than the DDG. The post-hydrolysis samples both show fewer crystalline components implying a more exfoliated surface than the pre-hydrolysis samples (confirmation of BET surface area data). Yet, the soy still shows some non-exfoliated portions that are defined by strong organizational lines. This is in comparison to the DDG sample, which appears to be almost completely exfoliated. Both contain quite a few layers of graphitic material but would still be considered amorphous. Diffraction patterns also showed typical carbon characteristics (Figure 4.6 b and d). While both pre and post-hydrolysis carbons showed

similar graphitic qualities, the higher level of exfoliation for post-hydrolysis samples make them better candidates in energy storage applications.

6. *Chemical Composition Studies*

Single line EDAX can provide chemical composition of materials. This composition was analyzed to see exactly how pure the material was in terms of its elemental composition. Figure 4.7 shows the resulting graphs and areas that were analyzed.

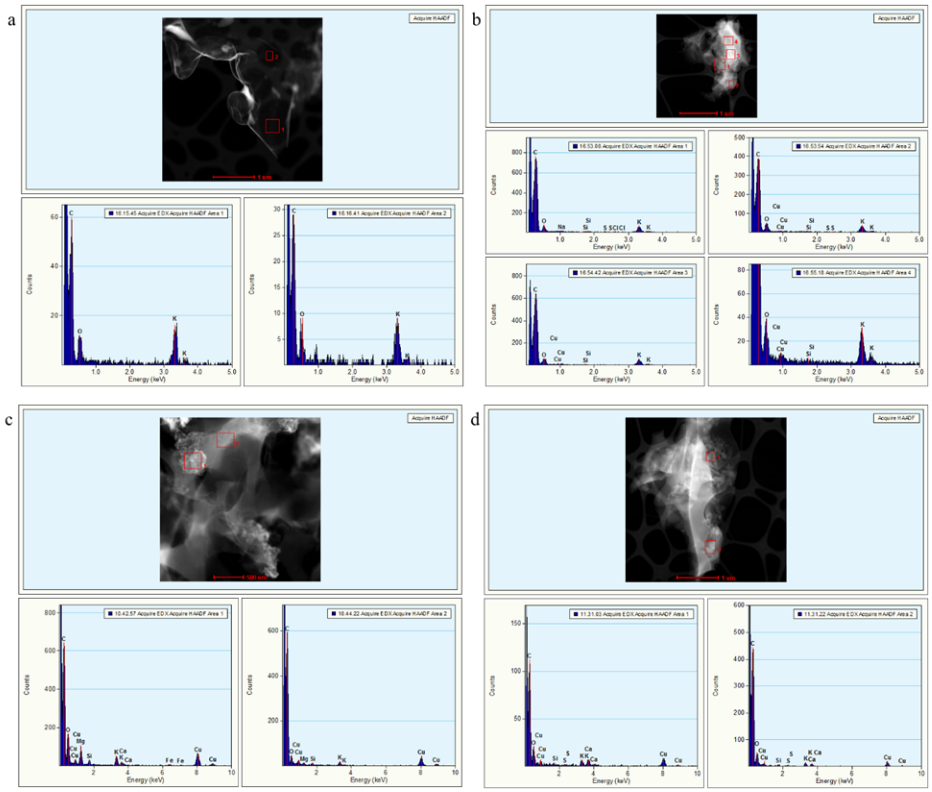

FIGURE 4.7 - Single line EDAX analysis of a) carbons made from pre-hydrolysis DDG, b) carbons made from post-hydrolysis DDG, c) carbons made from pre-hydrolysis soy hulls, and d) carbons made from post-hydrolysis soy hulls

As can be seen in the graphical counts provided underneath the images of the various carbons, elemental carbon dominates in all four samples ranging from 60-93% of the total atom counts. Oxygen and potassium were the next highest counts for the DDG, which can be explained by the activating agent used. This could be indicative of the washing procedure not being thorough enough and leaving behind residual material or of functional groups that result from the redox reactions that take place on the surface. Copper and calcium appear in the soy hulls. Calcium is understandable due to the higher levels of calcium found naturally in the soy hulls. The presence of copper is due to the mount on which the material is placed in the microscope. The presence of the calcium elements is minimal compared to the carbon, oxygen, and potassium atoms present in the samples. From this data, it can be gathered that there would possibly be some interference in charge transfer if the oxygen atoms were indeed part of functional groups.

7. *Raman Spectroscopy Studies*

Raman spectra were then obtained to help determine the structure and to compare the spectra to samples of commercially available activated carbons.

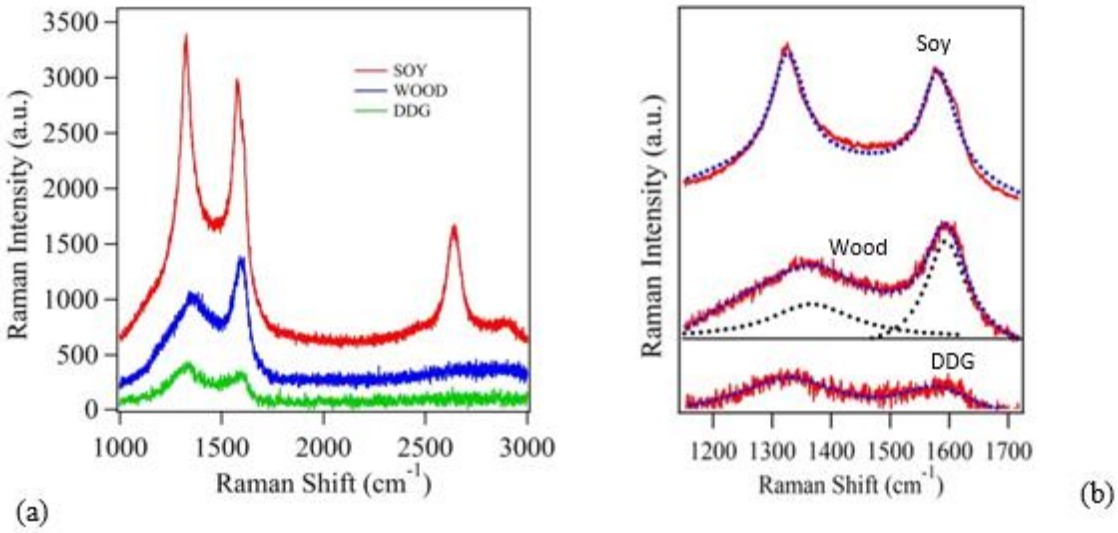

FIGURE 4.8 - Raman spectra of DDG, soy, and wood (control) carbon samples to compare organization of the carbon structure. (a) shows the entire spectrum while (b) focuses on the range containing the D and G peaks associated with carbonaceous materials

As shown in Figure 4.8 (a), all three of the spectra show traditional peaks found in most carbon results from literature. When discussing carbon materials, these spectra are divided into 3 main peaks; The G peak, which is found at 1580 cm^{-1} in disordered carbons [Dresselhaus, 2002], the D peak at 1350 cm^{-1}, and the 2D peak which represents an overtone of the vibration from the D peak at around 2690 cm^{-1} [Dresselhaus, 2002]. The presence of a D peak in all three samples and a G peak generally represent two different characteristics of the carbon structure. The D band representing bonds of disordered carbons, and the G band is representative of graphitic bonds. Figure 4.8 (b) shows the D

and G bands with Lorentzian curve fits to help remove noise from the data. The intensity ratio of the D and G bands calculated for all three samples were 0.21, 0.86, 1.25 for wood, DDG, and soy derived ACs respectively. The intensity ratio is related to the structure of carbon materials and is calculated using the peak heights of the D and G bands ($R=I_D/I_G$). The lower the intensity ratio, the lower the disorder of the materials. This would indicate that the MWV control sample has the lowest amount of disorder, followed by the DDG, and then the soy. For the soy derived sample, presence of a few layers of graphene is evident from the appearance of a strong 2D peak, but the layer stacking becomes imperfect causing a high intensity ratio, R. The structural parameter, L_a of the fibers is related to the intensity ratio, R as $L_a=C/R$, where C is a constant. From our Raman results it can be concluded that L_a is largest for the wood derived sample and smallest for soy derived samples. The D and G peaks confirm the carbonaceous nature of the carbons from soy, DDG, and wood and their applicability in energy storage applications.

C. APPLICATIONS OF CARBONS IN RENEWABLE ENERGY DEVICES

1. Electrochemical Storage in Supercapacitors

Electrochemical measurements were conducted for the use of ACs in a supercapacitor structure. Figure 4.9 (a) shows preliminary results of supercapacitor characteristics for both electrodes comprising high surface area AC (produced with 1:1 KOH activation) as the active material when the full cell is charged and discharged between 0 and 3.5 V at the current density of 500 mA/g. The electrolyte was 1.5 M TEAPF6-PC (Tetraethylammonium hexafluorophosphate in propylene carbonate).

S1: Control. Carbonized DDG, no KOH
S2: 0.17:1 KOH:DDG
S3: 0.17:1 KOH:DDG, fluffed fibers
S4: 1:1 KOH:DDG

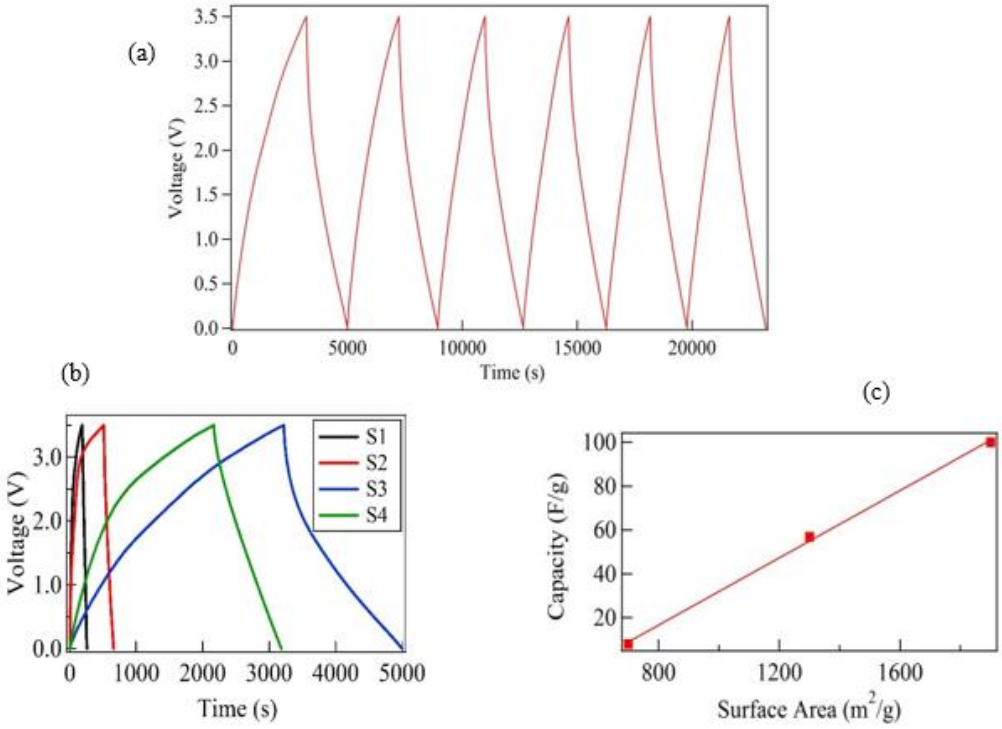

FIGURE 4.9 - Electrochemical performance of ACF samples measured in a 2032 coin-cell configuration system using 1.5 M TEAPF6-PC (Tetraethylammonium hexafluorophosphate in propylene carbonate) solution as the electrolyte. (a) Galvanostatic charge–discharge curves for sample S4 at 500 mA/g current density during first 6 cycles (b) Comparison of cycling performance of various ACF samples at current of 500 mA/g (c) capacitance vs. surface area

Near-linear voltage-time relation (discharge) is characteristic of an electric double layer capacitance. There is a slight distortion of the curves presumably caused by the pseudocapacitance of functional-groups. The discharge curve has a much steeper slope than the charge curve, meaning that the discharge occurs over a much shorter time. It must follow then that the power that the supercapacitor can provide would be greater than

supercapacitors with longer discharge times, as power is a ratio of energy to time. This carbon material can also charge and discharge at higher voltages, about 3.5 volts, which is higher than many standard devices. This also increases the power that the supercapacitor can provide as the power is proportional to the voltage squared (Equation 6).

$$P = \frac{\frac{1}{2}(CV^2)}{\Delta t} \tag{6}$$

The specific capacitance of the electrode was calculated by the equation,

$$C = \frac{I\Delta t}{m\Delta V} \tag{7}$$

where I, Δt, m, and ΔV are the applied current, discharge time, mass of the active material, and the voltage change, respectively. First cycle capacity was found to be ~ 100 F/g. Fig. 4.9 (b) compares the supercapacitor performance of the four samples produced with varying ratios of KOH (Table III) under same current density (500 mA/g) including the non-activated sample as the control (S1). The cycling performance of the AC increased dramatically as the surface area increased from S1 to S4. However, it cannot be only surface area that affects the capacitance as S3 (~740 m^2/g) has a larger integrated charge/discharge area than S4 (~1700 m^2/g). The capacitance value is seen to range from 4 F/g to 100 F/g. Fig. 4.9 (c) shows that the capacitance varied linearly with the

concentration of KOH, showing a correlation between the two. This variation of capacitance may stem from the fact that it has varying pore sizes compared to the triethylamine cation, TEA^+ and hexafluorophosphate anion, PF_6^- thereby affecting the effective accessibility of electrode/electrolyte interface areas. When the pores and the ions are able to match effectively, this can allow full utilization to form the double layer and contribute to the higher capacity value. Carbons that have high surface areas but low capacitances are typically found to be mesoporous materials, which yields poor matching between ions and pores in the system. Therefore, it is imperative to properly tune the pore size to match the ion size for high capacitances.

2. Carbon Electrode Perovskite Solar Cells

The carbons were used to construct perovskite solar cells in the manner described by Mei et. al (2014). During this process, sintering of the carbon electrodes occurs to solidify the layer onto the structure in addition to removing liquid that could disrupt the flow of electrons through the system. As a test, the carbons were screen printed onto FTO glass and then sintered at the required temperatures to see if they could hold up to the processing effectively. Upon removal of the carbon-coated glass from the sintering plates, it was found that the layers were not structurally sound and much of the material had burned off at the elevated temperatures. In the case of pure activated carbon, heat cannot destroy or burn activated carbons because of its stable form. The only explanation for this result is that there are functional groups on the surfaces that allow for oxidation of the material. These results would therefore seem to corroborate the pseudo capacitance denoted by the curvilinear charge/discharge graphs discussed in the previous section.

In an attempt to use the carbons in other parts of the device, the paste for the zirconium layer was made with approximately 10% by mass of the carbons. This was then incorporated into the standard construction of the device. Upon sintering of the zirconium layer, it was observed that, as in the electrode layer, the carbon in the zirconium paste also burned off during the sintering process. The device was completed and performance was compared to a standard device without carbon in the zirconium layer. Preliminary results showed that the device that had the carbon in the zirconium layer had higher photo-conversion efficiencies than the standard cells, increasing from 9-12%. The explanation for this centers around the removal of the carbon and the resulting structure that was left behind when those carbons were burned off. In theory, the zirconium layer has a higher surface area due to void space created when the carbons are burned off. This could allow for more direct contact and penetration of the perovskite through the carbon and into the zirconium layer. This direct connection of the light sensitive material to a conducting transport layer could explain the higher efficiencies. However, much more research would need to be performed to see if this hypothesis were true.

To see if the functional groups could be removed, they were washed in varying concentrations of inorganic acids and sintered in a similar manner to perovskite devices made previously. The differences in the masses of carbon pastes from a control sample and carbons washed with inorganic acids were measured before and after sintering. Percentage mass lost helped give a metric for how effective the cleaning procedures worked. From the preliminary data presented in Table V, cleaning with acids resulted in a lower mass loss than just washing with DI water at all temperatures tested. In these trials,

changing the sintering temperatures also provided some insight into the temperature effect on mass loss. Both sulfuric and nitric acid cleanings led to dramatic decreases in mass loss at all sintering temperatures. The nitric acid was the most effective at reducing mass losses to only 40 and 35 % (Table 5-3) at the actual sintering temperatures required for these specific devices. If the hypothesis about functional groups causing the burning of the carbons is true, then this would indicate that the acids removed these volatiles and that the resulting material could sinter without any issues and be used as intended in perovskite solar cell devices.

TABLE V

TABLE INDICATING THE PERCENTAGE CHANGES IN MASS BETWEEN CARBONS CLEANED WITH ACIDS AND CARBONS CLEANED WITH DI WATER

Acid Type	**Temperature ˚C**	**Initial Mass (g)**	**Mass with Paste (g)**	**Post-Sintering (g)**	**% Burned Off**
DI Water	300	1.484	1.505	1.486	90
Nitric Acid		1.53	1.537	1.532	71
Sulfuric Acid		1.628	1.636	1.63	75
DI Water	350	1.594	1.598	1.595	75
Nitric Acid		1.523	1.528	1.526	40
Sulfuric Acid		1.535	1.541	1.537	67
DI Water	400	1.584	1.589	1.584	100
Nitric Acid		1.533	1.55	1.544	35
Sulfuric Acid		1.527	1.532	1.528	80

This mass change is assumed to be mainly due to loss of moisture and carbon material. The larger the percentage difference, the less effective the cleaning procedure at removing oxidative groups.

3. *Hydrogen Storage Applications*

As described in the literature, solid-state hydrogen storage would be an effective way to use hydrogen in vehicles without the need to compress it to high pressures or use it as a liquid at extremely low temperatures. The Conn Center is developing a modular system that would involve depositing activated carbons onto a membrane and then rolling the membrane into a spiral shape. Gas would then flow through the center of the roll and would radiate out to fill the voids in the carbon. A variety of dispersion techniques were used to determine qualitatively if the deposition of carbons onto a membrane was possible. Table VI shows the changing ratios of oil to hexane that were used as the liquid in the carbon suspension. It then shows the correlating descriptions of the layers formed with each ratio of oil to hexane.

TABLE VI

QUALITATIVE CARBON LAYER FORMATION USING VARYING RATIOS OF OIL AND HEXANE TO DISPERSE CARBONS EFFICIENTLY ONTO A PTFE MEMBRANE

	Ratio Oil:Hexane by Mass			
Oil Type	1:0	3:1	1:1	1:3
Mineral Oil	Extremely slow filtration process with a solid carbon layer.	Liquid goes through membrane slowly but a more solid layer forms. Could be good for modular storage if it has the surface area.	Carrier solvent filters through quickly and leaves behind a brittle layer that doesn't stick well to the membrane.	Precise layer is formed with minimal processing time.
Sunflower Oil	Extremely slow filtration process with a solid carbon layer.	Liquid goes through membrane slowly, but faster than the mineral oil. A solid layer forms. Could be good for modular storage if it has the surface area.	Slower solvent filtration compared to the mineral oil, also leaves a brittle carbon layer.	Precise layer is formed with minimal processing time.

As expected, layers made with higher ratios of oil to hexanes resulted in slower processing, but layers that bound well together. This is the expected result of higher viscosity solutions that have minimal evaporation. In the case of the 3:1 ratios, the solution moves through the membrane more quickly as the solution is thinned by the added hexane. The sunflower oil solution passes through more quickly due to its lower viscosity and both form a layer that could be stable. In the 1:1 samples, the layer left behind becomes brittle, making it difficult to justify using for a storage module. The layer was not flexible enough to deal with membrane bending. Counter-intuitively, the mineral oil suspension filtered faster than the sunflower oil suspension with this ratio. This is

most likely explained by the volume of material used as the ratios were maintained, but differing overall masses could have affected the filtration. Finally, the 1:3 ratio suspensions formed precise layers quickly, and would probably be the best to experiment with going forward. Ultimately, the use of a specific ratio would be dependent on the surface area of the final module. Intuitively, the pure oil layers would clog pores and allow for little if any storage of gas. This surface area would slowly increase as the hexane amount increased. However, layers that break are unable to be measured. The best option would be to find the ideal ratio, then measure the surface area to see if it is justifiable for use in a hydrogen storage module.

D. TECHNO-ECONOMIC ANALYSIS OF CARBONS FROM DDG

Techno-Economic analysis was performed to demonstrate some preliminary revenue calculations from activated carbon production. In this particular case, the focus is on the carbon activation process specifically, not the biorefinery as a whole, in order to isolate it and make it transferrable from process to process. Table VII shows the profits obtained via the production of activated carbons for energy storage uses based on an industry price of $4000/tonne.

TABLE VII

REVENUES FROM CARBON PRODUCTION FOR ENERGY STORAGE DEVICES FROM DDG

DDG Entering (tonnes/yr)	**Residual Fiber (tonnes/yr)**	**Profit ($/yr)**
25000	5000	3770498.09
50000	10000	8155857.64
75000	15000	12541217.19
100000	20000	16926576.74
125000	25000	21311936.29
150000	30000	25697295.84
175000	35000	30082655.39
200000	40000	34468014.94
225000	45000	38853374.49
250000	50000	43238734.04
275000	55000	47624093.59
300000	60000	52009453.14
325000	65000	56394812.69
350000	70000	60780172.23
375000	75000	65165531.78
400000	80000	69550891.33
425000	85000	73936250.88
450000	90000	78321610.43
475000	95000	82706969.98
500000	100000	87092329.53

An increase in throughput of DDG fiber leads to a linear increase in revenue. In each of these cases, that revenue would ideally be used to assist with costs associated with the agricultural process to which it would be attached. Depending on the process specified, the range of revenue presented above could be used as a good estimate of the potential revenues for agricultural processing and biorefinery. For example, the initial range between 2,500 to 1 million tonnes of DDG/yr would probably be more

apt for beverage alcohol distillation. The higher amounts could easily be satisfied by bioethanol plants in the Midwest. Looking at the lowest initial DDG value, the impact can be broken down to see the effects on processing costs at an hourly basis. Assuming 50 operating weeks and 22 operating hours per day, the revenue provided from the carbons made from 25000 tonnes of DDG per year is approximately $500 per hour that could go toward lowering the price of the units of material being made. The volume of units produced per hour could then be used to calculate the price effect per unit, lowering the cost of a gallon of bioethanol or a bottle of bourbon by that amount.

V. CONCLUSION

The main objective presented in this work was to create a value-added co-product from residual fiber in a C-5 biorefinery process. At a processing temperature of 950 °C, increases in activating agent concentration (KOH) led to increased surface areas. 0:1, 0.17:1, and 1:1 mass ratios of KOH to DDG fiber yielded carbons that had BET surface areas ranging from 0.47 m^2/g to 1700 m^2/g. The pore widths from these samples varied from 8.39 nm to 2.08 nm with the addition of KOH. These surface area and pore width changes correlated positively with the amount of KOH present in the sample, confirming literature data.

SEM imaging of the pre and post-hydrolysis fibers showed that there was a dramatic surface difference when the C-5 sugars were removed. The resulting carbons made from these fibers then showed that the hydrolysis process had a major impact on the surface areas of the resulting carbons. Carbons made from pre-hydrolysis DDG only reached BET surface areas of 10.44 m^2/g while carbons made from post-hydrolysis DDG reached as high as 1705 m^2/g. The surface areas of the carbons made from pre and post-hydrolysis soy hulls increased from 689 m^2/g to 1316 m^2/g. In terms of the pore sizes, pre and post-hydrolysis DDG had average pore widths of 9.5 and 2.9 nm respectively while pre and post-hydrolysis soy hulls had average pore widths of 2.7 and 2.2 nm respectively. These values were improvements over current wood-based industrial carbons.

TEM imaging showed that the carbons made from pre-hydrolysis fibers, while graphitic in nature, had large crystalline sections and showed lesser organization than the post-hydrolysis samples. The diffraction patterns of all four samples radiated out from the

material in two circular bands which is expected for carbonaceous materials. Single line EDAX showed that carbon was the main constituent of all of the materials with slight amounts of oxygen and potassium from the activating agent.

In supercapacitors, capacitances increased from 4 F/g to 100 F/g with increasing surface area, where 100 F/g is considered a relatively good capacitance for smaller electronic devices. Cycling of the samples showed that cycling efficiency increased with increasing surface area. However, the data also indicated that this efficiency was not directly correlated to surface area and could have more to do with pore size or another parameter.

Screen-printed layers of carbon that would be used in perovskite devices were found to be unstable and burned upon sintering. This quality was then used in the zirconium layer of a perovskite device to increase the surface area of said layer. This modification increased device efficiency from 9-12% compared to a control. Inorganic acids were then used as cleaning solutions, and heat testing on the carbon samples showed that cleaning with acids improved heat stability at varying temperatures. Nitric acid was found to be the most effective washing agent as the carbons washed with it lost only 35% total mass at 400 °C compared to 80% for the carbons washed with sulfuric acid and 100% for the carbons washed with DI water alone.

A ratio of 1:3 mass of oil to mass of hexane could quickly create an even layer for hydrogen storage modules. An increase in oil mass led to slow processing time.

Techno-economic analysis showed (without initial capital costs) that profits ranged from $3.8 million for 5000 tonnes of residual DDG fiber processed annually to

$87 million for 100000 tonnes of residual DDG processed annually. This savings could directly drive down processing costs.

VI. RECOMMENDATIONS

Optimization of the carbonization procedure in terms of temperature and length of time could help improve economics; temperatures as low as 500 °C can be used for carbonization purposes with heating times as short as 30 minutes [Wang, 2012]. Some time and temperature tests could reduce the overall energy cost, but could also sacrifice carbon quality. Cleaning the carbons in an efficient manner or producing carbons in such a manner that removes any functional groups that impact the stability of the material would be of benefit as well. Some methods are already being explored, including the washing of the carbons with an acid solution. Another method to consider would be plasma processing, using low energy plasma to remove surface groups. In terms of characterization, more detail could be obtained by investigating more biomass species that are prevalent in different geographical areas. In theory, the implementation of this biorefinery concept before carbonization could prove useful on many forms of biomass with high hemicellulose content. Other characterization, such as crystallography or x-ray diffraction, could quantify the structure of the carbons more effectively. From these methods, the crystal structure could reveal whether the carbons form more of a 3-D or 2-D structure. This information can then provide better matching of the materials with their applications and allow for better tuning of the procedure depending on eventual use. In terms of the applications, use of devices that use supercapacitors would be a logical next step to the supercapacitor data obtained in these experiments. Hybrid vehicles, consumer electronics, and military satellite technology are just a few of the many applications for supercapacitors. Comparison to current technology in these applications could then help determine whether or not they are worth using in everyday devices. For the perovskite

solar cells, removal of functional groups is key. Once a cleaning process is established that creates stable carbon materials, the devices could be made with these stable carbons and then tested as before. This would ideally lead to working devices. For the hydrogen storage modules, work needs to continue to look toward a membrane layer that maintains the porosity required to adsorb hydrogen. Modeling with standard CFD would allow for simulation of the hydrogen through the membrane apparatus and then physical modules could be constructed based on the results from these simulations. The testing of temporary binders that would disintegrate at elevated temperatures could also be explored. Polymeric materials such as ethyl cellulose could provide the dispersion needed for a proper layer and then be removed to yield better surface areas. Economic analysis would need to include estimations of equipment costs and payback periods based on capacity. This data would allow for a more thorough cost benefit analysis which could help determine the minimum capacity required for a plant to operate this process to obtain revenue to aid in their biorefinery economics.

REFERENCES

Ahluwalia, Rajesh, T. Q. Hua, J. K. Peng, S. Lasher, Kurtis McKenney, and J. Sinha. "Technical Assessment of Cryo-Compressed Hydrogen Storage Tank Systems for Automotive Applications." (2009): n. pag. Web.

Andrieu, X. Energy Storage Syst. Electron.: New Trends Electrochem. Technol. 1 (2000) 521.

Bae, Dong-Ho, Sae-Rom Park, Sang-Do Ha, Ji-Ho Yoon, Sung-Yong Lee, Kwon-Pyo Hong, Eun-Hye Lee, Hye-Jung Yeom, Nam-Gyoon Yoon. "Exposure to Ethyl Carbamate in Alcohol-drinking and Nondrinking Adults and Its Reduction by Simple Charcoal Filtration."*Food Control* 20.10 (2009): 946-52. Web.

Becker, H.I., Low voltage electrolytic capacitor, United States Patent 2,800,616 (1957).

Beguin, F., et al. "Carbons with narrow pore size distribution prepared by simultaneous carbonization and self-activation of tobacco stems and their application to supercapacitors." *Carbon* 81 (2015): 148-157.

Brunauer, Stephen, P. H. Emmett, and Edward Teller. "Adsorption of Gases in Multimolecular Layers." *Journal of the American Chemical Society* 60.2 (1938): 309-19. Web.Burke

Campbell, Neil A., Jane B. Reece, Lisa A. Urry, Michael L. Cain, Steven Alexander Wasserman, Peter V. Minorsky, and Rob Jackson. *Campbell Biology*. 10th ed. San Francisco: Benjamin Cummings, 2013. Print.

Cardona, Carlos A., and Óscar J. Sánchez. "Fuel Ethanol Production: Process Design Trends and Integration Opportunities." *Bioresource Technology* 98.12 (2007): 2415-457.

Carrott, P. J. M., Suhas, and M.M.L. Ribeiro Carrott. "Lignin - from Natural Adsorbent to Activated Carbon: A Review." *Bioresource Technology* 98.12 (2007): 2301-312. Web.

Dias, Joana M., Maria C.m. Alvim-Ferraz, Manuel F. Almeida, Jose Rivera-Utrilla, and Manuel Sanchez-Polo. "Waste Materials for Activated Carbon Preparation and Its Use in Aqueous-phase Treatment: A Review." *Journal of Environmental Management* 85.4 (2007): 833-46. Web.

Do, D. D. and A. Ahmadpour "The preparation of active carbons from coal by chemical and physical activation." *Carbon* 34.4 (1996): 471-479.

Dresselhaus, M.s., G. Dresselhaus, A. Jorio, A.g. Souza Filho, and R. Saito. "Raman Spectroscopy on Isolated Single Wall Carbon Nanotubes." *Carbon* 40.12 (2002): 2043-061.

Fonseca, Dania A., Robert Lupitskyy, David Timmons, Mayank Gupta, and Jagannadh Satyavolu. "Towards Integrated Biorefinery from Dried Distillers Grains: Selective Extraction of Pentoses Using Dilute Acid Hydrolysis." *Biomass and Bioenergy* 71 (2014): 178-86. Web.

Frackowiak, Elzbieta, and Francois Beguin. "Carbon Materials for the Electrochemical Storage of Energy in Capacitors." *Carbon* 39 (2001): 937-50. Print.

Gercel, Ozgul, and H. Ferdi Gercel. "Adsorption of Lead(II) Ions from Aqueous Solutions by Activated Carbon Prepared from Biomass Plant Material of Euphorbia Rigida." *Chemical Engineering Journal* 132.1-3 (2007): 289-97. Web.Graetz

Graetzel, Michael. "The Light and Shade of Perovskite Solar Cells." *Nature Materials* 13.9 (2014): 838-42. Web

Graetzel, Michael, Seigo Ito, Peter Chen, Pascal Comte, Mohammad Khaja Nazeeruddin, Paul Liska, and Peter Pechy. "Fabrication of Screen-printing Pastes from TiO2 Powders for Dye-sensitised Solar Cells." *Progress in Photovoltaics: Research and Applications* 15.7 (2007): 603-12. Web.

Hameed, B. H., and A. A. Rahman. "Removal of Phenol from Aqueous Solutions by Adsorption onto Activated Carbon Prepared from Biomass Material." *Journal of Hazardous Materials*160.2-3 (2008): 576-81. Web.

H. von Helmholtz, Ann. Phys. (Leipzig) 89 (1853) 211.

Hurter, R. E. 2007. Non-wood fiber raw materials and the biorefinery. TAPPI EPE Conference, Jacksonville, FL, October 21-24.

Idris, Juferi, Yoshihito Shirai, Yoshito Andou, Ahmad Amiruddin Mohd Ali, Mohd Ridzuan Othman, Izzudin Ibrahim, Akio Yamamoto, Nobuhiko Yasuda, and Mohd Ali Hassan. "Successful Scaling-up of Self-sustained Pyrolysis of Oil Palm Biomass under Pool-type Reactor." *Waste Management & Research* 34.2 (2016): 176-80. Web.

Jüntgen, H. "Activated carbon as catalyst support: a review of new research results." *Fuel* 65.10 (1986): 1436-1446.

Karagoz, S., T. Tay, S. Ucar, and M. Erdem. "Activated Carbons from Waste Biomass by Sulfuric Acid Activation and Their Use on Methylene Blue

Adsorption." *Bioresource Technology*99.14 (2008): 6214-222. Web.Kazi, F. K., Fortman, J. A., Anex, R. P., Hus, D. D., Aden, A., Dutta, A., Kothandaraman, G. Techno-economic comparison of process technologies for biochemical ethanol production from corn stover. *Fuel* 89 (2010): 520-528.

Kirk, Raymond, Donald Frederick Othmer, Jaqueline E. Kroschwitz, Mary Howe-Grant. "Biomass Energy." Kirk-Othmer: Encyclopedia of Chemical Technology. Vol. 3. New York: Wiley-Interscience, 2007. 683-707. Print.

Kojima A., K. Teshima, Y. Shirai and T. Miyasaka, *J. Am. Chem. Soc.*, 2009, 131, 6050-6051.

Langmuir, Irving. "The Adsorption Of Gases On Plane Surfaces Of Glass, Mica And Platinum."*Journal of the American Chemical Society* 40.9 (1918): 1361-403. Web.

Lillo-Rodenas, M. A., D. Cazorla-Amoros, and A. Linares-Solano. "Understanding Chemical Reactions between Carbons and NaOH and KOH: An Insight into the Chemical Activation Mechanism." *Carbon* 41 (2003): 267-75. Print.

Linares-Solano, A., et al. "Influence of pore size distribution on methane storage at relatively low pressure: preparation of activated carbon with optimum pore size." *Carbon* 40.7 (2002): 989-1002.

Lotfabad, Elmira Memarzadeh, et al. "High-density sodium and lithium ion battery anodes from banana peels." *Acs Nano* 8.7 (2014): 7115-7129.

Lupitskyy, Robert, Charles Staff, and Jagannadh Satyavolu. "Towards Integrated Biorefinery from Dried Distillers Grains: Evaluation of Feed Application for Co-products." *Biomass and Bioenergy* 72 (2015): 251-55.

McEnaney, B., T.D. Burchell (Eds.), Carbon Materials for Advanced Technologies, *Pergamon*, 1999, p. 1

Mitlin, David, Jia Ding, Huanlei Wang, Zhi Li, Kai Cui, Dimitre Karpuzov, Xuehai Tan, and Alireza Kohandehghan. "Peanut Shell Hybrid Sodium Ion Capacitor with Extreme Energy-power Rivals Lithium Ion Capacitors." *Energy Environ. Sci.* 8.3 (2015): 941-55. Web.

Mitzi, D. B. *Synthesis, Structure and Properties of Organic–Inorganic Perovskites and Related Materials: Progress in Inorganic Chemistry* Vol. 48 (ed. Karlin, K. D.) 1–121 (J. Wiley & Sons, 1999).

Mohamed, Abdul Rahman, Norhusna Mohamad Nor, Lee Chung Lau, and Keat Teong Lee. "Synthesis of Activated Carbon from Lignocellulosic Biomass and Its

Applications in Air Pollution Control-a Review." *Journal of Environmental Chemical Engineering* 1.4 (2013): 658-66. Web.

Møller, C. K. *Nature* **182,** 1436 (1958).

Namasivayam, C., and D. Kavitha. "Removal of Congo Red from Water by Adsorption onto Activated Carbon Prepared from Coir Pith, an Agricultural Solid Waste." *Dyes and Pigments*54.1 (2002): 47-58. Web.

National Academies Press, The Hydrogen Economy: Opportunities, Costs, Barriers, and R&D Needs, National Research Council Report, 2004, p. 44, available at: http://www.nap.edu/catalog/10922.html. (2004).

Pandolfo, A.g., and A.f. Hollenkamp. "Carbon Properties and Their Role in Supercapacitors." *Journal of Power Sources* 157.1 (2006): 11-27. Web.

Pauling, L. *General Chemistry*. Dover Publications. New York, New York (1947): 169. Print.

Perlack, Robert D., Lynn Wright, Anthony Turhollow, and Robin L. Graham. "Biomass as Feedstock for a Bioenergy and Bioproducts Industry: The Technical Feasibility of a Billion-Ton Annual Supply." USDA and USDOE Technical Report. April 2005. Web.

Pierson, H. O., Handbook of Carbon, Graphite, Diamond and Fullerenes, Noyes Publications, NJ, USA, 1993.

Ponseca, C. S. *et al. J. Am. Chem. Soc.* **136,** 5189–5192 (2014).

Quantum Fuel Systems Technologies Worldwide Project Report, FY 2005 Annual Progress Report for the DOE Hydrogen Program, November 2005, available at: http://www.hydrogen.energy.gov/annual_progress05_storage.html.

Rightmire, R. A., Electrical energy storage apparatus, United States Patent 3,288,641 (1966).

Rouquerol, J., Philip Llewellyn, and F. Rouquerol, "Is the BET Equation Applicable to Microporous Adsorbents?." *Studies in Surface Science and Catalysis*. 160 (2007): 49-56. Web.

Sandia National Laboratories Project Report, FY2005 Annual Progress Report for the DOE Hydrogen Program, November 2005, available at: http://www.hydrogen.energy.gov/annual_progress05_storage.html

Satyapal, Sunita, John Petrovic, Carole Read, George Thomas, and Grace Ordaz. "The U.S. Department of Energy's National Hydrogen Storage Project: Progress towards Meeting Hydrogen-powered Vehicle Requirements." *Catalysis Today* 120.3-4 (2007): 246-56. Web.

Savaliya, Mehulkumar L., Bhaveshkumar D. Dhorajiya, and Bharatkumar Z. Dholakiya. "Recent Advancement in Production of Liquid Biofuels from Renewable Resources: A Review." *Research on Chemical Intermediates* 41.2 (2013): 475-509. Web.

Shukla, A. K., S. Sampath, and K. Vijayamohanan. "Electrochemical supercapacitors: Energy storage beyond batteries." *CURRENT SCIENCE-BANGALORE*- 79.12 (2000): 1656-1661.

Shukla, A. K., *Resonance* 6 (2001) 72.

Solomon, Barry D., Justin R. Barnes, and Kathleen E. Halvorsen. "Grain and Cellulosic Ethanol: History, Economics, and Energy Policy." *Biomass and Bioenergy* 31.6 (2007): 416-25.

Spiccia,, Leone, Yu Han, Steffen Meyer, Yasmina Dkhissi, Karl Weber, Jennifer M. Pringle, Udo Bach, and Yi-Bing Cheng. "Degradation Observations of Encapsulated Planar CH3NH3PbI3 perovskite Solar Cells at High Temperatures and Humidity." *J. Mater. Chem. A*3.15 (2015): 8139-147. Web.

Stephenson RR. Crash-induced fire safety issues with hydrogen-fueled vehicles: http://www.hydrogensafety.info/articles/RhoadsStephensonpaper.pdf; 2004.

Stoumpos, C. C., Malliakas, C. D. & Kanatzidis, M. G. *Inorg. Chem*. **52,** 9019–9038 (2013).

Stranks, S. D. *et al. Science* **342,** 341–344 (2013).

Thommes, Matthias. "Physisorption of Gases, with Special Reference to the Evaluation of Surface Area and Pore Size Distribution (IUPAC Technical Report)." *Chemistry International*38.1 (2016): Web.

United States Department of Energy Annual Energy Outlook, 2006, available at: http://www.eia.doe.gov/oiaf/aeo/ (accessed February 2017)

United States Department of Energy, Office of Energy Efficiency and Renewable Energy. “Hydrogen, Fuel Cells & Infrastructure Technologies Program Multi-Year Research, Development and Demonstration Plan.” available at: http://www.eere.energy.-gov/hydrogenandfuelcells/mypp. (2005) (accessed February 2017)

United States Department of Energy, Office of Energy Efficiency and Renewable Energy. “Integrated Biorefineries.” https://www.energy.gov/eere/bioenergy/integrated-biorefineries (accessed February 2017).

Utgikar, Vivek P., and Todd Thiesen. "Safety of Compressed Hydrogen Fuel Tanks: Leakage from Stationary Vehicles." *Technology in Society* 27.3 (2005): 315-20. Web.

Van, Khu Le, and Thu Thuy Luong Thi. "Activated Carbon Derived from Rice Husk by NaOH Activation and Its Application in Supercapacitor." *Progress in Natural Science: Materials International* 24.3 (2014): 191-98. Web.

Wang, Huanlei, Zhanwei Xu, Alireza Kohandehghan, Zhi Li, Kai Cui, Xuehai Tan, Tyler James Stephenson, Cecil K. King’Ondu, Chris M. B. Holt, Brian C. Olsen, Jin Kwon Tak, Don Harfield, Anthony O. Anyia, and David Mitlin. "Interconnected Carbon Nanosheets Derived from Hemp for Ultrafast Supercapacitors with High Energy." *ACS Nano* 7.6 (2013): 5131-141. Web.

Wang, Jiacheng, and Stefan Kaskel. "KOH Activation of Carbon-based Materials for Energy Storage." Journal of Materials Chemistry 22 (2012): Print.

Weber, D. *Z. Naturforsch.* 33b**,** 1443–1445 (1978).

Wells, H. L. *Z. Anorg. Chem*. 3, 195–210 (1893).

Xing, G. C. *et al. Science* 342**,** 344–347 (2013).

Yoon, Seong-Ho, Seongyop Lim, Yan Song, Yasunori Ota, Wenming Qiao, Atsushi Tanaka, and Isao Mochida. "KOH Activation of Carbon Nanofibers." *Carbon* 42 (2004): 1723-729. Print.

Zuttel A. Hydrogen storage methods. *Naturwissenschaften* 2004; 91 p.157–72. Web.

APPENDIX A

Parameters

Material and Energy Balances	**Per Year**		
	Cost	Units	
DDG	100	$/tonne	USDA
KOH	300	$/tonne	Alibaba
Water	0.00203	$/gallon	LWC
Energy Balance	30800000	Kwh	LG&E
4000 Watts	0.0682	$/kwh	
350 working days	2100560	$/yr	
22 hours/day			
Carbon Yield	0.42		
Carbon Cost	4000	$/tonne	Alibaba
Cp Nitrogen	1157	kJ/tonne-K	Eng Toolbox
Cp DDG	1600	kJ/tonne-K	Eng Toolbox
Cp KOH	1170	kJ/tonne-K	Eng Toolbox
DDG Density	0.240277	tonne/m3	UGA
Nitrogen Density	0.0003309	tonne/m3	Peace Software
At 1.2 atm			
Start Up Energy Cost	Mass (tonnes)	Temperature Change	Heats of Fusion (MJ/tonne)
DDG	10	600	NA
KOH	10	600	120
Energy Required (kWh)	Cost		Pyrolysis Oil is used to
2666688	181868.1216		Heat any dryers and
1950048.934	132993.3373		Heaters
	314861.4589		
Operators	3		
$-yr/operator	300000		
Pyrolysis Oil HV	20	MJ/L	btg-btl.com

Material and Energy Balances based on given parameters

DDG Entering	Residual Fiber (tonnes)	Volume DDG	KOH (tonnes)	Water (gallons)	$ DDG	$ KOH	$ Water	Materials Cost
25000	5000	20809.31591	5000	7160000	2500000	1500000	14534.8	4014534.8
50000	10000	41618.63183	10000	14320000	5000000	3000000	29069.6	8029069.6
75000	15000	62427.94774	15000	21480000	7500000	4500000	43604.4	12043604.4
100000	20000	83237.26366	20000	28640000	10000000	6000000	58139.2	16058139.2
125000	25000	104046.5796	25000	35800000	12500000	7500000	72674	20072674
150000	30000	124855.8955	30000	42960000	15000000	9000000	87208.8	24087208.8
175000	35000	145665.2114	35000	50120000	17500000	10500000	101743.6	28101743.6
200000	40000	166474.5273	40000	57280000	20000000	12000000	116278.4	32116278.4
225000	45000	187283.8432	45000	64440000	22500000	13500000	130813.2	36130813.2
250000	50000	208093.1591	50000	71600000	25000000	15000000	145348	40145348
275000	55000	228902.4751	55000	78760000	27500000	16500000	159882.8	44159882.8
300000	60000	249711.791	60000	85920000	30000000	18000000	174417.6	48174417.6
325000	65000	270521.1069	65000	93080000	32500000	19500000	188952.4	52188952.4
350000	70000	291330.4228	70000	100240000	35000000	21000000	203487.2	56203487.2
375000	75000	312139.7387	75000	107400000	37500000	22500000	218022	60218022
400000	80000	332949.0546	80000	114560000	40000000	24000000	232556.8	64232556.8
425000	85000	353758.3705	85000	121720000	42500000	25500000	247091.6	68247091.6
450000	90000	374567.6865	90000	128880000	45000000	27000000	261626.4	72261626.4
475000	95000	395377.0024	95000	136040000	47500000	28500000	276161.2	76276161.2
500000	100000	416186.3183	100000	143200000	50000000	30000000	290696	80290696

Nitrogen Volume (m3)	Nitrogen mass (tonnes)	Energy Input (kWh)	Energy Cost	Carbon Produced (tonnes)	Carbon Revenue	Profit
41618.63183	13.77160527	1549.126714	105.6504419	2100	8400000	3770498.09
83237.26366	27.54321054	3098.253427	211.3008838	4200	16800000	8155857.64
124855.8955	41.31481582	4647.380141	316.9513256	6300	25200000	12541217.19
166474.5273	55.08642109	6196.506855	422.6017675	8400	33600000	16926576.74
208093.1591	68.85802636	7745.633569	528.2522094	10500	42000000	21311936.29
249711.791	82.62963163	9294.760282	633.9026513	12600	50400000	25697295.84
291330.4228	96.40123691	10843.887	739.5530931	14700	58800000	30082655.39
332949.0546	110.1728422	12393.01371	845.203535	16800	67200000	34468014.94
374567.6865	123.9444475	13942.14042	950.8539769	18900	75600000	38853374.49
416186.3183	137.7160527	15491.26714	1056.504419	21000	84000000	43238734.04
457804.9501	151.487658	17040.39385	1162.154861	23100	92400000	47624093.59
499423.5819	165.2592633	18589.52056	1267.805303	25200	100800000	52009453.14
541042.2138	179.0308685	20138.64728	1373.455744	27300	109200000	56394812.69
582660.8456	192.8024738	21687.77399	1479.106186	29400	117600000	60780172.23
624279.4774	206.5740791	23236.90071	1584.756628	31500	126000000	65165531.78
665898.1093	220.3456844	24786.02742	1690.40707	33600	134400000	69550891.33
707516.7411	234.1172896	26335.15413	1796.057512	35700	142800000	73936250.88
749135.3729	247.8888949	27884.28085	1901.707954	37800	151200000	78321610.43
790754.0048	261.6605002	29433.40756	2007.358396	39900	159600000	82706969.98
832372.6366	275.4321054	30982.53427	2113.008838	42000	168000000	87092329.53

VITA

Zachary Dean Herde was born on August 26, 1993 in Louisville, KY and has lived there ever since. After being inspired to pursue a career with a chemistry focus by both his high school chemistry teacher, Mrs. Alice Hall, and Mr. Alton Brown (of Food Network fame), he started pursuing chemical engineering at the University of Louisville as a James Graham Brown Fellow in the Fall of 2012. Since then, he has been actively involved in research with the Conn Center for Renewable Energy Research as part of the Biomass and Biofuels Group under the tutelage of Dr. Jagannadh Satyavolu. Here his research focused on integrated biorefinery and value-added co-products. Through the Conn Center, he also worked in the Laboratory of Photonics and Interfaces under Drs. Michael and Carole Graetzel at the École Polytechnique Fédérale de Lausanne in Lausanne, Switzerland where he learned about the theory and manufacturing of perovskite solar devices. After receiving his Bachelor's in August of 2016, he began the Master of Engineering program in Chemical Engineering with a certification in Environmental Engineering.

An avid musician, Zachary performed with the University of Louisville Wind Ensemble, Cardinal Pride Pep Band, Holy Name Band of Louisville, and the Louisville Winds. In addition, he is an Eagle Scout and Assistant Scoutmaster for his troop, Troop 314 of St. Matthews, Kentucky. He was a 5-year member of the Library Student Advisory Board, treasurer and president of the Mortar Board Honor Society, and was named a Kentucky Colonel by the Governor of Kentucky in April of 2016.

In the Fall of 2017, he plans to pursue a doctoral degree in chemical engineering from the School of Chemical and Biomolecular Engineering at the Georgia Institute of Technology in Atlanta, Georgia.